December 1986 LIDS-P-1629

Phase Unwrapping of Signals Propagated Under the Arctic Ice Crust: A Statistical Approach[§]

José M. F. Moura[†]
and
Arthur B. Baggeroer[‡]

Abstract: The paper studies the phase unwrapping of time signals transmitted under the Arctic ice crust. Unexpected phase discontinuities observed in a previous study [14] of the same data prompted the need for a robust phase unwrapper. The acoustic source generates a narrowband sequence whose phase experiences random fluctuations. At the receiving hydrophones, the measurements are corrupted by wideband noise. With this formulation, the reconstruction of the random phase fits naturally the setting of statistical signal processing [16]. We apply discrete optimal nonlinear filtering techniques [5] to design the phase unwrapping algorithm. The scheme presented proves more insensitive to noise than other nonstatistical unwrappers, supporting less stringent prefiltering constraints. Under the conditions of the Arctic experiment, it accomodates processing of each individual sensor's output data, avoiding the need for beamforming. Also, to discriminate between intrinsic phenomena and transients induced by the prefilters, shorter duration impulse responses are desired. Accordingly, the prefilters are designed with large bandwidths, the statistical unwrapper withstanding satisfactorily the lower signal to noise ratio environment. To take advantage of this flexibility, the data are processed under alternative conditions which assume different values for the statistical parameters. The similarities of the corresponding unwrapped phase paths help to discriminate those rapid events which are intrinsic from those which are artifacts introduced by the processing. By using real signals that travelled several hundred kilometers through a highly unstable channel, the work shows that nonlinear statistical designs are viable and useful in many practical problems of underwater acoustics.

§Work supported by the Office of Naval Research, Arctic Program Office, under research contract no. N00014-86-K-0325. The processing reported here and the text preparation used computational facilities made available by the Laboratory for Information and Decision Systems (MIT), sponsored by the Army Research Office under contract DAAG-29-84-K-005.

†Department of Electrical and Computer Engineering, Carnegie-Mellon University; the work was carried out while with the Department of Electrical Engineering and Computer Science and LIDS, Massachusetts Institute of Technology (visiting), on leave from Instituto Superior Técnico, Lisbon, Portugal.

‡Department of Electrical Engineering and Computer Science, Massachusetts Institute of Technology.

1. Introduction

The present work studies the phase of continuous wave acoustic signals after being transmitted several hundred kilometers under the ice crust in the Arctic Ocean. It develops phase unwrappers that take into account the statistical nature of the signals. For low signal to noise ratios, these unwrappers prove more robust to phase jumps than other phase unwrapping algorithms. The motivation for the study stems from the presence of phase discontinuities on a previous analysis of the same signals in [14]. The statistical phase unwrapper allows for greater flexibility in terms of the actual processing. Without noticeable performance degradation it accomodates processing of the data of each individual sensor, prior to array beamforming, as well as preprocessing filters with larger bandwidths and shorter impulse response durations. This is particularly relevant when it is desired to discriminate which phase discontinuities exhibited by other phase unwrappers are intrinsic or are the result of processing artifacts.

The actual data collection experiments have been described previously, see [8], [2], [3]. They are part of an ongoing research program started in 1977, which include onsite data gathering missions in the Arctic, e.g., the Fram 2 (1980) expedition, the Fram 4 (1982), the Marginal Ice Zone Experiment MIZEX 83, MIZEX 84, and the forthcoming Winter MIZEX (1987). In [14], data collected under Fram 2 showed unexpected and unexplained phase discontinuities. The difficulty with the phase unwrapper of [14] lies in its sensitivity to the noise levels. To rule out possible processing deficiencies, a new phase estimator is presented here that exhibits a high degree of flexibility and resists to phase jumps under low signal to noise ratios.

In section 2, we give a brief description of the underlying data measuring experiments, summarizing previous processing experience. The conceptual question of phase unwrapping is considered in several distinct aspects in sections 3 to 6. Section 3 overviews the problem. Section 4 presents the statistical phase unwrapper. Section 5 details its implementation, as a compromise of performance vis a vis complexity. This is an adaptation of the algorithm in [10], [11] to the signal processing problem under consideration here. Section 6 analyses the phase unwrapper behavior under controlled conditions (simulated study in a digital computer). Finally, section 7 applies the statistical phase unwrapper to the Arctic data. The preprocessing required is examined there, and the robustness to poor prior statistical knowledge used to further resolve questions about the nature of fast phase changes.

The paper shows that more sophisticated algorithms can be used in the context of many underwater acoustics experiments. The prefiltering required by the statistical algorithms is also present in the more classical approaches. Focusing on feature extraction, the preprocessing cleans the data of background noise in outband signal components, smoothing its (over) sampled values. Highly tuned prefilters, e.g., narrow band pass or low pass filters, array beamforming, etc., may on the other hand mask the data with manmade artifacts. Extending the signal to noise ratio threshold of good performance, the statistical procedure places less stringent

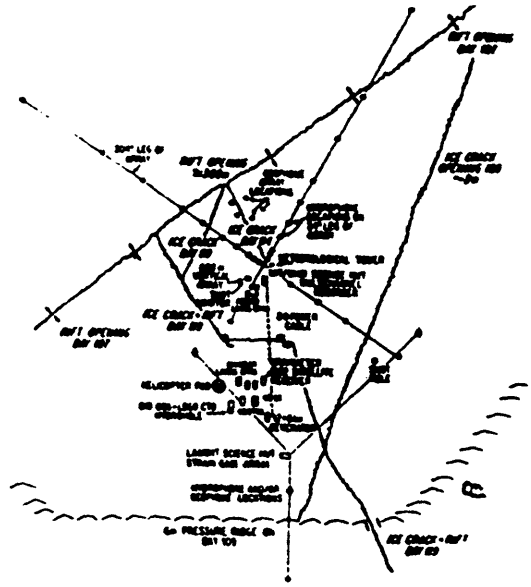

Figure 1. Camp layout at Fram 2 with the location of the array of hydrophones (not to scale).

constraints on the preprocessing schemes, reducing the chance of contamination of the raw data by spurious events. The price paid is in terms of sophistication, and hence of computer power needed. However, as argued later on, simple minded approximations to optimal approaches translate in reasonable compromises that obtain most of the performance gain available, at a cost which requires only a fractional increase of the processing complexity. To the authors' knowledge, the present is the first published account of the use of nonlinear stochastic filters in a real world problem. That the data have propagated and were collected under severe conditions, just strengthens the belief that these techniques should find in the future a wider utilization.

2. Data Collection Experiments in the Arctic Ocean

The research program Fram 2 was conducted from ice stations on drifting pack ice from March 19, 1980 to May 5, 1980. It concentrated on underwater acoustics, marine geophysics, and physical oceanography in the eastern Arctic Ocean. Fram 2 was the second of a series of four manned, drifting ice stations in the Eurasion Basin of the Arctic Ocean. The scientific program for Fram 2 was described in [8]. It involved three ice stations – a main camp, Fram 2, and two remote sites. See figure 1 for the camp layout and scientific equipment at Fram 2. The camp was approximately 2 km by 2 km. It included a 22-channel array of hydrophones, a four-channel geophone array, an ocean bottom seismometer (OBS), a gravimeter, two satellite navigation receivers, as well as a host of other probes and sensors for physical oceanographic measurements.

The hydrophone elements were suspended to a depth of 91 m through holes drilled in the ice. The interelement spacing was log periodic, and the overall dimensions were approximately 800 m on each leg of an L shaped array. Subsequent ice breakup forced redeployment into an X shape. The data from the hydrophones were recorded on a multichannel digital data acquisition system. Each hydrophone was monitored separately, digitized at a 250-Hz sampling rate, and recorded on magnetic tape. The principal scientific equipment at camps 1 and 2 was controllable mechanical sources for transmitting low-frequency, moderate power, coherent acoustic signals to the Fram 2 camp during the acoustic transmission component of the program. Specifically, the signals we are concerned here originated at camp 1, about 343 km to the north of Fram 2. They consisted of tones centered at 15 Hz. The source was a Hydro-acoustics HLF-3 operated at a depth of 91 m. The peak power was 165 to 177 dB re 1μPa at 1 m. The receiving system response rolled off above 80 Hz. The disturbances were very low frequency noise of mechanical origin, wideband omnidirectional noise in the 1-80 Hz band, and a 60 Hz interference. See [2] for further details.

The Fram 2 tonal data have been extensively analyzed in [14]. The sequence of processing tasks to unwrap the phase included beamforming with a standard delay and sum technique, decimation by a factor of 2, quadrature demodulation, low pass filtering using a 500 point finite impulse response (FIR) digital filter, rolling off from 0 dB at .016 Nyquist to -50 dB at .024 Nyquist. At the .008 s sampling interval, the cutoff frequency is 1 Hz. The quadrature demodulated data were further decimated by a factor of 16, low pass filtered again to obtain a 128 mHz passband centered on the demodulated tone (cutoff at 64 mHz). Finally, the demodulated data were analyzed by spectral and statistical techniques. The phase sequence was reconstructed by unwrapping on the line the arctan of the quadrature components of the filtered signal, see section 3. Although the received signal is composed of many single paths travelling under the ice crust, the analysis in [14] concludes that the fluctuations of the single path vectors is negligible compared with the noise. A suitable model is then, in polar coordinates, to assume that the total envelope amplitude ρ is a vector sum of a constant signal vector and a noise vector whose quadrature components are Gaussian. The statistical tests carried out consubstantiated this hypothesis, which again underlies the model to be presented in section 4. Only two deep fades were identified, both in the same experiment, one larger than $>$ 20dB, and the other of 5 dB. The fade durations were very short, less than 1 min. The corresponding phase skips observed in the phase unwrapped path were however intriguing in that they did not correspond to full cycle skips. Questions remained about the true nature of these events. The phase demodulated scheme used did not endure shorter FIRs, or larger filter bandwidths, or individual processing of the single hydrophones. The design of a more reliable phase unwrapper resisting noisier environments, is then important to help clarifying possible causes for these anomalies.

3. Phase Unwrapping of Discrete Time Signals

Phase unwrapping of discrete time signals (DTS) is important in many signal processing applications, from speech to geophysics or underwater acoustics. In the communications field, it is known as phase demodulation. Given a complex valued time series $x[n], n = 0, 1, \ldots$, the phase is constructed as the continuous sequence

$$\tan(\widetilde{\phi}[n]) = \frac{\Im m\{x[n]\}}{\Re e\{x[n]\}}. \tag{3-1}$$

Of course, the difficulty lies in that the available no memory subroutine computing the inverse tangent function to recover $\widetilde{\phi}[n]$ from (3–1) only contributes to the so called principal value of the phase, i.e., its value modulo 2π. Several authors have studied the problem of phase unwrapping. We consider only the question of phase unwrapping of time signals, not that of the Fourier spectrum. In [13] and [4], the problem is addressed by looking at the shifted version of $\widetilde{\phi}[n]$ that suitably accounts for a multiple number of shifts of $\pm\pi$, depending on the zero crossings of $\Re e\{x[n]\}$. To avoid a global dependence on possible local errors resulting from incorrect identification of these zeros, an algorithm using Sturm sequences is developed in [13] and applied in [4] to symmetric and anti-symmetric sequences.

The models underlying the phase unwrapping algorithms discussed in the literature do not account for two features that are present in the data of many signal processing applications of interest. Namely, that the measurements of $x[n]$ are compounded and corrupted by noise, and that the phase itself may be a random sequence. Bringing this to bear has several implications. On one hand, the problem becomes harder, it lies in the realm of stochastic filtering with nonlinear signals. On the other hand, the noisy nature of the involved signals is taken into consideration, consequently a more robust phase estimate is to be expected. Formulating the problem in this framework allows the development of a statistical phase unwrapping algorithm that is conceptually simple and that eliminates most of the induced phase jumps. The algorithm combines, in an optimal statistical sense, the information provided by the data sequence and the *prior* information regarding the constraints the data should satisfy. A reasonable model considers for example the phase as a second order process where the second order differences are independent identically distributed (iid) Gaussian random variables. Higher order models are incorporated with no added difficulty. As it turns out, reliable performance is achieved even for poor prior knowledge on the statistical noises' power levels. The algorithm constructs estimates for the phase and its first (and higher) order time differences (depending on the model assumed). It is designed via the (discrete time) stochastic nonlinear filtering theory. The theory provides a nonlinear recursive scheme that updates, via Bayes' law, the probability distribution function (PDF) of the phase process (and its higher order differences) given the measurements. If the phase has values in the field of the reals (not digitized), the algorithm requires the time propagation of a function taking values in a continuous interval of the real line. For actual computation in a finite resource environment, finite representations of this function

are required. Except in trivial applications, no finite representation can capture the complete description of the function, approximations being mandatory. The next two sections describe the design theory of optimal discrete nonlinear filtering and its practical implementation in the context of the problem under study.

4. A Statistical Phase Unwrapping Algorithm

The phase process is assumed to be the output of a linear discrete time invariant (LDTI) system driven by independent, identically distributed (iid) Gaussian random variables with spectral level q, as in figure 2. We write

$$\phi[n+N] + a_{N-1}\phi[n+N-1] + \cdots + a_0\phi[n] = b_N u[n+N] + \cdots + b_0 u[n]. \quad (4\text{–}1)$$

Figure 2. Linear Discrete Time Invariant System.

Some or all of the $a_i, i = 0, \ldots, N-1$, and some or all but one of the $b_j, j = 0, \ldots, N$, may be zero. We assume random initial conditions to start (4–1). We take

$$\phi[0], \ldots, \phi[N-1]$$

to be jointly Gaussian random variables, independent of the $\{u[n]\}$, for all n. The constant amplitude signal process is

$$\begin{aligned} \tilde{x}[n] &= \sqrt{2P}\exp\{j\phi[n]\} \\ &= x_c[n] + jx_s[n]. \end{aligned}$$

The measurements are

$$\tilde{z}[n] = \tilde{x}[n] + \tilde{w}[n],$$

with

$$\begin{aligned} \tilde{w}[n] &= W_n \exp\{j\theta_n\} \\ &= w_c[n] + jw_s[n] \end{aligned}$$

where $\{w_c[n], w_s[n]\}$ are zero mean iid Gaussian random variables with spectral level r, independent of $\{u[n]\}$ for every n, and independent of the initial phase values or the initial data. We actually work with real signals, and let

$$z[n] = \begin{bmatrix} z_1[n] \\ z_2[n] \end{bmatrix}$$

where $z_1[n] = \widetilde{z}_c[n], z_2[n] = \widetilde{z}_s[n]$. Similarly for $x[n]$ and $w[n]$. Introduce the normalized noise to signal ratio σ in the filter band

$$\sigma = \frac{r \cdot W}{P} \tag{4–2}$$

where W is the filter equivalent (half) bandwidth.

With the above notation, two possible phase estimate sequences can be constructed. One is the (first component of the) mean of the conditional predicted PDF

$$P_n[\Lambda] = \Pr\{\lambda \leq \Lambda \mid z[0], \ldots, z[n-1]\}$$

and the other is the mean of the filtered PDF

$$F_n[\Lambda] = \Pr\{\lambda \leq \Lambda \mid z[0], \ldots, z[n]\}\,.$$

To compute the conditional mean phase $\widehat{\phi}[n]$ one needs to propagate the PDF's P_n and F_n. This is provided by Bayes' law, e.g., [5]. Without going into the details, we concentrate on the two steps of the algorithm itself:

Prediction Step:

$$P_n = F_{n-1} * Q_n \tag{4–3}$$

Filtering Step:

$$F_n = P_n \bullet H_n\,. \tag{4–4}$$

In (4–3), the predicted PDF P_n at time n is obtained by a convolution $(*)$ operation of the filtered PDF F_{n-1} available at time $n-1$ and a Gaussian kernel Q_n corresponding to the PDF of the iid random variables $\{u_n\}$. In (4–4), a pointwise multiplication $(\bullet)$ of P_n with a Gaussian kernel H_n (the PDF of the random variables $\{w_n\}$) constructs F_n at time n. Actually, step (4–4) is accomplished usually in two substeps

$$F_n^1 = P_n \bullet \widetilde{H}_n \tag{4–5a}$$

$$F_n = F_n^1 \times K_n \tag{4–5b}$$

where

$$\widetilde{H}_n(\Lambda) = \exp\left\{\frac{-\left(z_1[n]\cos\Lambda + z_2[n]\sin\Lambda\right)}{2r}\right\} \tag{4–5c}$$

is a periodic unnormalized kernel. Equation (4–5b) is a normalization procedure that guarantees F_n remains a PDF with

$$K_n = \frac{1}{\int F_n^1[d\Lambda]}. \tag{4–5d}$$

The filtered phase estimate sequence is constructed recursively by (4–3) to (4–5) and from

$$\widehat{\phi}[n] = \int \Lambda F[d\Lambda]. \tag{4–6}$$

The underlying model enters in the specific form of Bayes' law, equations (4–3) to (4–5). Because the support of the densities P_n and F_n is the real line $\Re^1$, the estimate provided by (4–6) takes values in $\Re^1$. The unwrapping of the phase sequence is accomplished directly by statistical means. The equivalent statement in continuous time follows from the continuity with respect to time of the solutions of differential equations. When noise disturbes the measurements, and in particular for high noise to signal power ratios, the fact that the noise is accounted for by the model and taken into consideration by the receiver design explains why the algorithm resists many of the phase jumps experienced by other techniques. This will be elaborated upon later on. The tradeoff may lie in the complexity of equations (4–3) and (4–5). This is certainly true when they are compared with a straightforward unwrapper (see section 3), being the price paid for better performance. It is questionable however, that the statistical phase unwrapper is significantly more complex than the unwrappers of [4] or [13]. As discussed in the next section, the implementation of the filter may be quite simple, and may still achieve most of the performance gain available. Hence, the interest of the present algorithm to many underwater signal processing applications.

5. Implementation of the Statistical Phase Unwrapper

In a digital environment, propagating (4–3) to (4–5) requires a finite representation of the functions involved, namely $F_n(\Lambda)$ and $P_n(\Lambda)$, as well as the Gaussian kernels $H_n(\Lambda)$ and $Q_n(\Lambda)$. Unfortunately, except in special cases, a complete description cannot be obtained by finite means. This implies that approximations be made, with consequent inherent resulting errors. The implementation of the algorithm must then strike a balance between the complexity of the solution and the errors one is willing to accomodate. Of course, the same question arises in many other fields, e.g., integration of partial differential equations (PDE). In a sense, (4–3)–(4–5) are nothing but the integral type solution of a parabolic PDE. We will not dwell into these analogies. But they serve to illustrate that a differencing (implicit) grid scheme is one possible representation method, the algorithm reducing then to the propagation of the discretizing grid and of the probability mass on the mesh points. The advantages of these procedures relate to the uniform flow of their computations, which, when tied to certain machine architectural constraints, may be exploited to speed up the algorithm. By just reducing the grid mesh, they also provide a simple way of controlling the corresponding numerical errors. The disadvantage lies on the associated computational effort. For higher order phase models, this effort may prove overwhelming when the filter is to be implemented in conventional serial hardware. For a summary of these issues see [6], [7].

We take here an alternative route that explores the specifics of the phase unwrapping problem. The algorithm is adapted to the present signal processing problem from the phase demodulator developed in [10], [11]. Recall that the class of Gaussian functions is closed under convolution and pointwise multiplication. Gaussian functions are completely described by their first and second order moments. If we represent F_n, P_n, H_n, and Q_n by finite sums of weighted Gaussian functions, each cycle of the algorithm just propagates the set of means, covariances, and weights associated with each function. The equations propagating the means and covariances are nothing but the discrete Kalman-Bucy filter equations [9]. The idea of using Gaussian functions for nonlinear filter implementation dates back to [1]. However, the implementation discussed here is different, particularly simple, and highly tailored to the phase problem.

A more careful analysis shows that there are two main difficulties. The first is that for a linear phase model, as a function of Λ, Q_n is Gaussian, but H_n, or $\widetilde{H}_n$, is not. So, each iteration does require a Gaussian approximation to H_n. The second results from the explosive growth on the required number of associated Gaussian basis functions. Multiplying or convolving N_1 Gaussians with N_2 Gaussians results into $N_1 N_2$ Gaussians. For a linear phase model, only the multiplication step increases the number of Gaussian functions. These two remarks are of a different nature. One is a representation issue, that of H_n by a Gaussian train. The second is of a projection type – maintaining the number of basis functions within a preset limit. The simplicity of the approach resides exactly on how to resolve satisfactorily these two questions. We address briefly both.

Representation of $\widetilde{H}_n$: Being periodic, the algorithm substitutes $\widetilde{H}_n$ by a train of Gaussians, where each Gaussian matches $\widetilde{H}_n$ at three points – a maximum and two neighboring preset values of $\widetilde{H}_n$. It is straightforward to show that $\widetilde{H}_n$ is completely described by two parameters: the location of one of its maxima provided by

$$\mu_n^H(0) = \arctan \frac{z_2[n]}{z_1[n]} \tag{5–1}$$

and by the common variance σ_n^H of all its Gaussian modes. A simple computation leads to

$$\sigma_n^H = \frac{\pi^2}{8 \,||\, z[n] \,||}\sigma \tag{5–2}$$

where $||\, z[n] \,|| = \sqrt{z_1^2[n] + z_2^2[n]}$, and σ was defined in (4–2). The algorithm represents $\widetilde{H}_n$ by a periodic sequence of equal variance Gaussian functions centered in (5–1).

Equation (5–1) evaluates the principal value of the phase process, if no observation noise corrupts the sensor measurements. It can still be looked upon as the best one shot ML-estimate of the (principal value) of the phase. Equation (5–2) gives the variance associated with the sensor measurement noise. It reveals a

simple minded but efficient adaptation to the assumed noise to signal power level σ. If at data point n the noise is weak,

$$|| z[n] || \approx 1$$

as it should be, and σ_n^H is a normalization of σ. If the noise annihilates one or both of the sensor measurements, $|| z[n] ||$ is small, and σ_n^H is large. The net effect is that the algorithm pays little attention to that point. One can also see that the algorithm misbehaves when due to noise

$$|| z[n] || \gg 1.$$

In actual practice, this can be taken into consideration with a hard limiter.

In the sequel, we will refer to the Gaussian components of each expansion as a Gaussian mode and represent mode i as $G(i)$. Optional superscripts F, P, H identify the function of which $G(i)$ is a mode.

Projection: With a linear phase model, the increase in the number of modes results at the filtering step. The projection is then applied at this stage of the algorithm, being accomplished in three phases:

i) Truncation: Each Gaussian mode G^P of P_n is multiplied by only the J most adjacent modes of $\widetilde{H}_n$. If N_n^P and N_n^F are respectively the number of Gaussian modes of P_n and F_n,

$$N_n^F = J \times N_n^P.$$

ii) Agglutination: Modes $G_n^F(i)$ and $G_n^F(j)$ which are close to each other

$$|| G_n^F(i) - G_n^F(j) || < \beta \qquad (5\text{–}3)$$

are agglutinated. In equation (5–3), β is a preset value. Agglutination of Gaussian functions is a Gaussian function, whose mean, variance and weight are easily evaluated from the corresponding values of the combined modes. Testing componentwise equation (5–3) requires for a 2-dimensional phase process two constants β_1 and β_2.

iii) Elimination: Mode $G_n^F(i)$ is eliminated if its weight $K_n^F(i)$

$$K_n^F(i) < \epsilon$$

where ϵ is a small positive number. This constraint is equivalent to bounding the maximum number of modes by $1/\epsilon$. Practice shows that usually the average number of modes is well under this limit.

Besides the statistical parameters, constants J, $\beta_i, i = 1,2$, and ϵ are needed. By prior experimentation, these are tuned to the particular application under study. If they are chosen so that N_n^F results on the average too small, the filter is on a predictive mode, transients may be missed. If they lead to N_n^F being too large, the algorithm relies heavily on new data, the filtering behavior prevails, the estimates are wigglier, the long term (local) mean square error behavior deteriorates. The details are not further pursued, the interested reader being refered to [12]. Figure 3 illustrates in block diagram the overall structure of the algorithm.

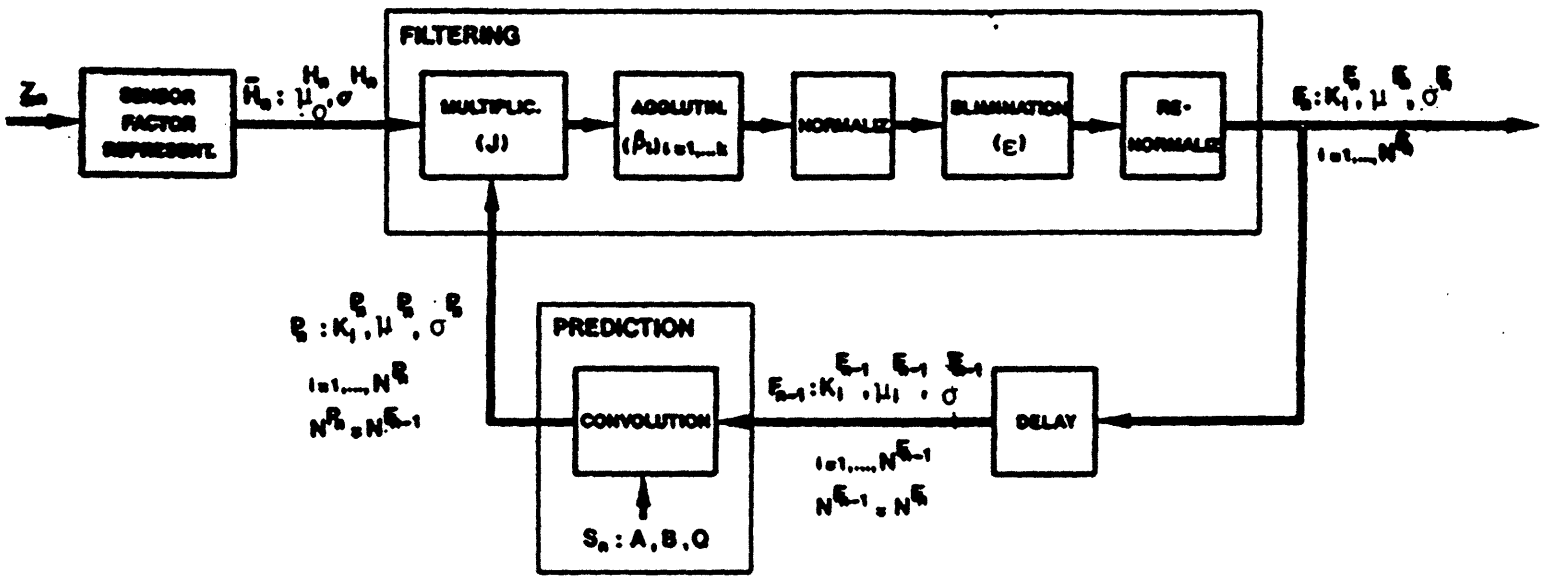

Figure 3.Statistical Phase Unwrapper Diagram.

6. Behavior Analysis Under Controlled Simulated Conditions

Due to the lack of analytical tools, the performance of nonlinear statistical filters is hard to analyse. In the context of several communications systems, extensive simulated studies of the algorithm presented in the last two sections have been carried out in [11]. However, the models used in engineering are simplifications of the real world. Errors arise from small offsets of the values assumed for unknown parameters with respect to their true values, or from structural mismatches between the model and the physical system. To understand how the phase unwrapper behaves under different operating conditions, the results of a controlled experiment are reported here. The simulated conditions try to emulate the Arctic data, from a noise to signal ratio point of view. Keeping in mind the objectives of section 7, the emphasis is on the qualitative behavior of the algorithm. In this and next sections, the acronyms SPW and APW are used to refer to the statistical phase unwrapper, and to the arctan phase unwrapper, respectively.

The simulations generated a chirp signal of the type used to improve resolution in radar systems. This choice is made because of its nonstationary character and its high frequency contents. Also, it helps understanding the tracker's behavior when the signal moves out of the filter band, see experiment 3 below. The phase rate is nominally linear in time. It has an added random component. The phase signal is

$$\phi[n] = 2\pi\frac{\alpha_0}{2}\Delta^2 n^2 + 2\pi f_0 \Delta n + \phi[0] + \varsigma[n]$$

where α_0 is the chirp constant, f_0 is the frequency offset, Δ is the sampling interval, and $\varsigma[n]$ is the random component. Letting,

$$\Lambda^1[n] = \phi[n]$$
$$\Lambda^2[n] = \frac{\phi[n+1] - \phi[n]}{\Delta}$$

and

$$\Lambda[n] = \left[\Lambda^1[n]\ \Lambda^2[n]\right]^T,$$

a suitable second order difference equation modeling the phase process is

$$\Lambda[n+1] = \begin{bmatrix} 1 & \Delta \\ 0 & 1 \end{bmatrix} \Lambda[n] + \begin{bmatrix} 0 \\ 1 \end{bmatrix} 2\pi\alpha_0\Delta + \begin{bmatrix} 0 \\ 1 \end{bmatrix} \Delta u[n] \qquad (6\text{–}1)$$
$$\Lambda[0] = \begin{bmatrix} \phi[0] \\ 2\pi f_0 \end{bmatrix}.$$

The set $\{u[n]\}, n > 0$, corresponds to a sequence of iid Gaussian random variables with zero mean and power level q. The observations are

$$y[n] = \sqrt{2P}\cos\phi[n] + \text{noise}. \qquad (6\text{–}2)$$

The preprocessing is illustrated in figure 4 and recovers the low pass components of (6–2)

$$z[n] = \sqrt{P}\begin{bmatrix}\cos\phi[n]\\ \sin\phi[n]\end{bmatrix} + \begin{bmatrix}w_c[n]\\ w_s[n]\end{bmatrix} \tag{6–3}$$

where P is the signal power. The sequence of iid Gaussian vectors

$$w[n] = [\,w_c[n]\, w_s[n]\,]^T$$

has zero mean, (double sided) spectral level of $r/2$, and is independent of the sequence $\{u[n]\}$.

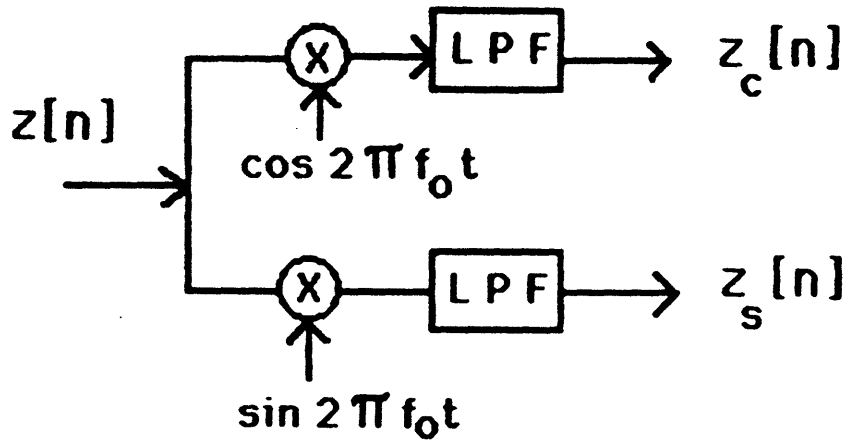

Figure 4. Preprocessing: Low Pass Quadrature Components.

A sequence of experiments was carried out where the response of the SPW is studied. For comparison, the phase path obtained by the APW is also considered. For all figures shown:

Signal and Noise:

Δ=sampling interval=0.008 s.
T=data span=20 s.
P=signal power=$8 \times 10^{-8}\mathrm{V}^2/\mathrm{s}$.
W=system input bandwidth=50 Hz.
α_0=chirp parameter=$0.5/\mathrm{s}^2$.
f_1=frequency shift=0 Hz.

Stochastic Phase Unwrapper (SPW):

J=truncation constant=3.
β_i=agglutination parameters=0.01, i=1,2.
ϵ=elimination parameter=0.01.

Depending on the experiment. combination of the following were adopted for the signal and noise:

f_0=tonal frequency=1 Hz; 15 Hz.

r=noise variance=$5 \times 10^{-9}; 5 \times 10^{-8}\mathrm{V}^2$

q=phase noise variance=0.1; $0.5\mathrm{V}^2$.

In many runs the algorithm was given erroneous values for some of the parameters. The preprocessing consisted of quadrature demodulation with a frequency equal to the nominal tone, followed by low pass filtering. Details are described next.

Experiment 1: q=0.1; r=5×10^{-9}.

Figure 5a shows the time series of the received waveform. Although not stationary, the Burg spectrum (5 poles used) in figure 5b provides an estimate of the frequency contents of the signal. After quadrature demodulation, the filter of figure 6 low pass filters the data. It is an FIR filter with an impulse response duration of 400 ms, i.e., extending over 50 samples. Its bandwidth of about 25 Hz is large enough to pass all the signal components. The filter is not made narrower so that the conditions of next section, where the preprocessing is to be as simple as possible, are best replicated. Figure 7 superimposes the phase paths of the true process (a), of the SPW (b), and of the APW (c). It is clear that the APW has lost track, while the SPW holds well the noisy environment, its phase estimate being almost undistinguishable from the true process. Also, the SPW provides an estimate for the phase rate, which is shown in figure 8 with the real phase rate.

Experiment 2: $f_0 = 15\mathrm{Hz}; q = 0.5; r = 5 \times 10^{-9}$.

In this experiment besides the higher frequency, the phase noise variance is boosted up. Figure 9 shows the Burg spectral estimate (10 poles). The frequency contents of the signal extends from 15 to 25 Hz, as expected from the value of the chirp parameter α_0=0.5, and of the total signal duration T=20 s. Figures 10 and 11 repeat for the present experiment figures 7 and 8, confirming the observations made above.

Experiment 3: $f_0 = 15\mathrm{Hz}; q = 0.5; r = 5 \times 10^{-8}$.

The signal values are as in the previous example, the noise level is increased by 10 dB. The noise is now of the same strength of the signal. This experiment is targeted to show how the SPW behaves when there are misfits in the model. The low pass prefilter used is shown in figure 12, with a cutoff frequency at approximately 5 Hz. At the midpoint of the data span, the chirp signal falls outside the filter band. In the first half of the observation interval, at the input of the SPW there are signal and noise. In the second half, the signal is missing, resulting in a basic inconsistency between the model and the (simulated) real world. The SPW was run several times over the same data, each run being fed with a different set of assumed values of the chirp parameter α_0, and of the phase noise variance q. Figures 13 and 14 display the phase and phase rate results. In the first half of the record, there is a reasonable agreement between all estimates and the true process, irrespectively of the offsets in the parameters. In the second part, the SPW exhibits a remarkable behavior. It is apparent that each SPW follows a different path. The absence of the signal being unknown to the algorithm, the data being the same, it is concluded that the filter follows in the second half of the observation interval, a path which is principally

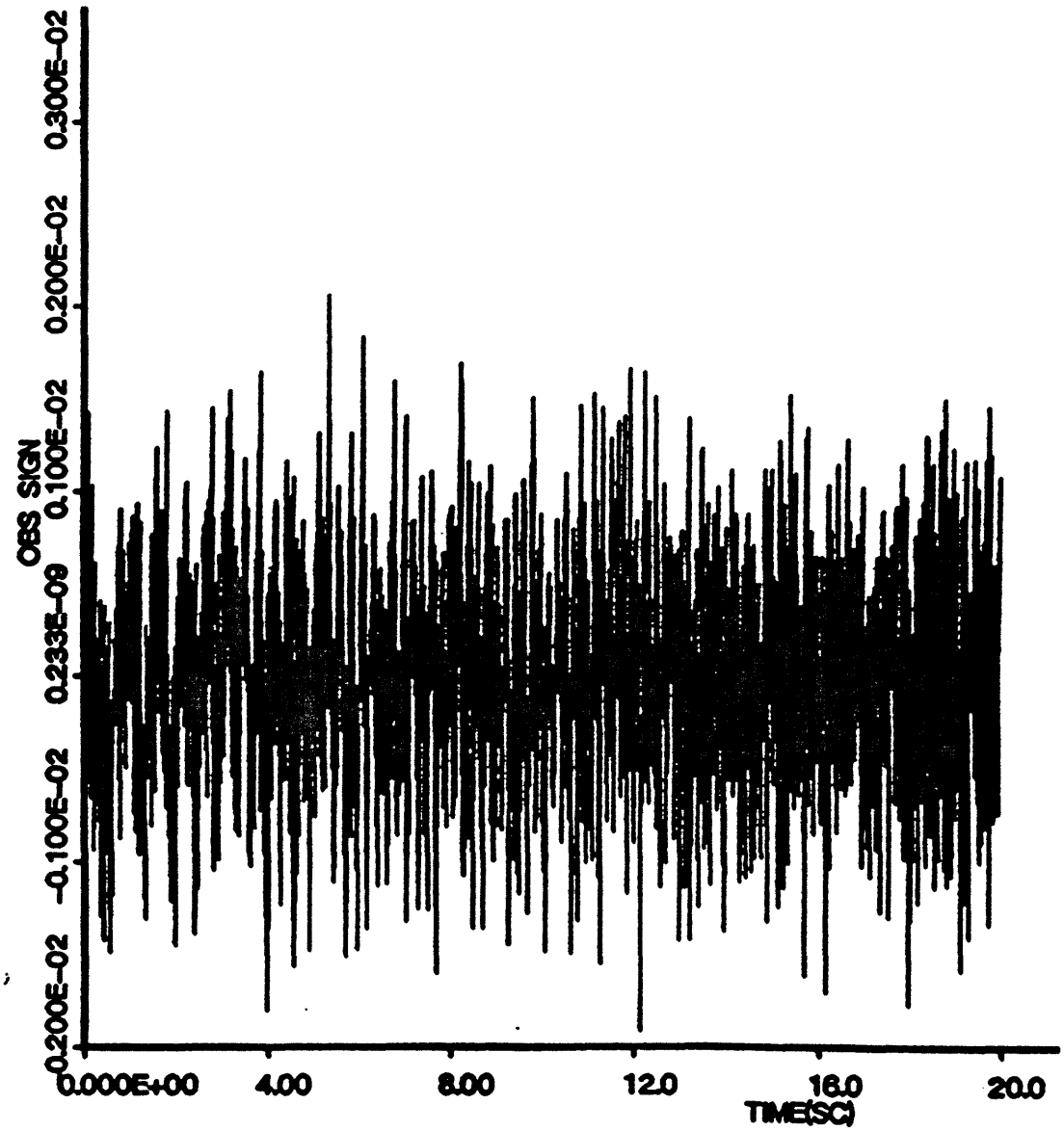

Figure 5a. Experiment 1 ($f_0 = 1\text{Hz} q = 0.1; r = 5 \times 10^{-9}$): Noisy Chirp Signal.

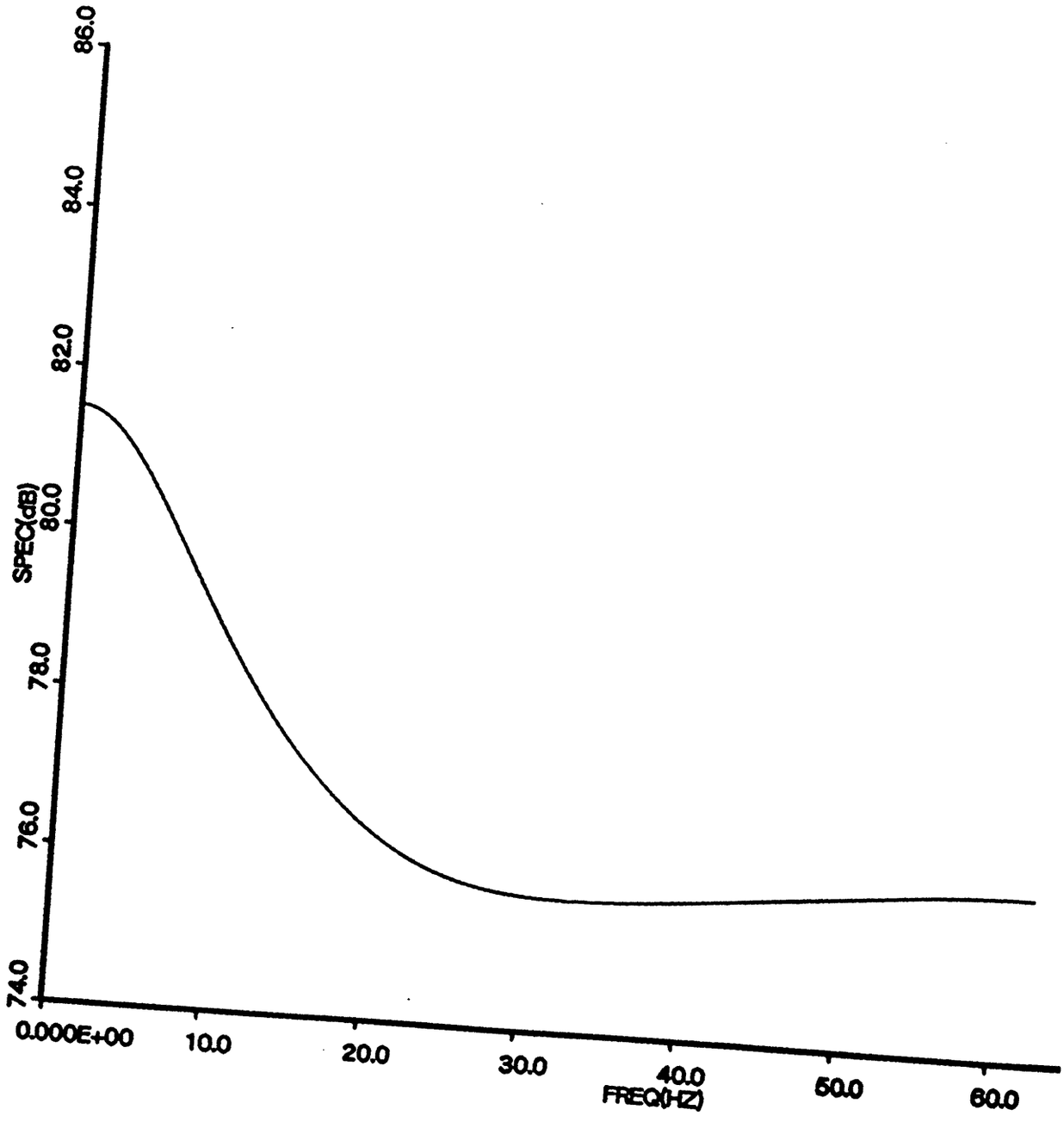

Figure 5b.Experiment 1: Burg Spectrum (5 poles).

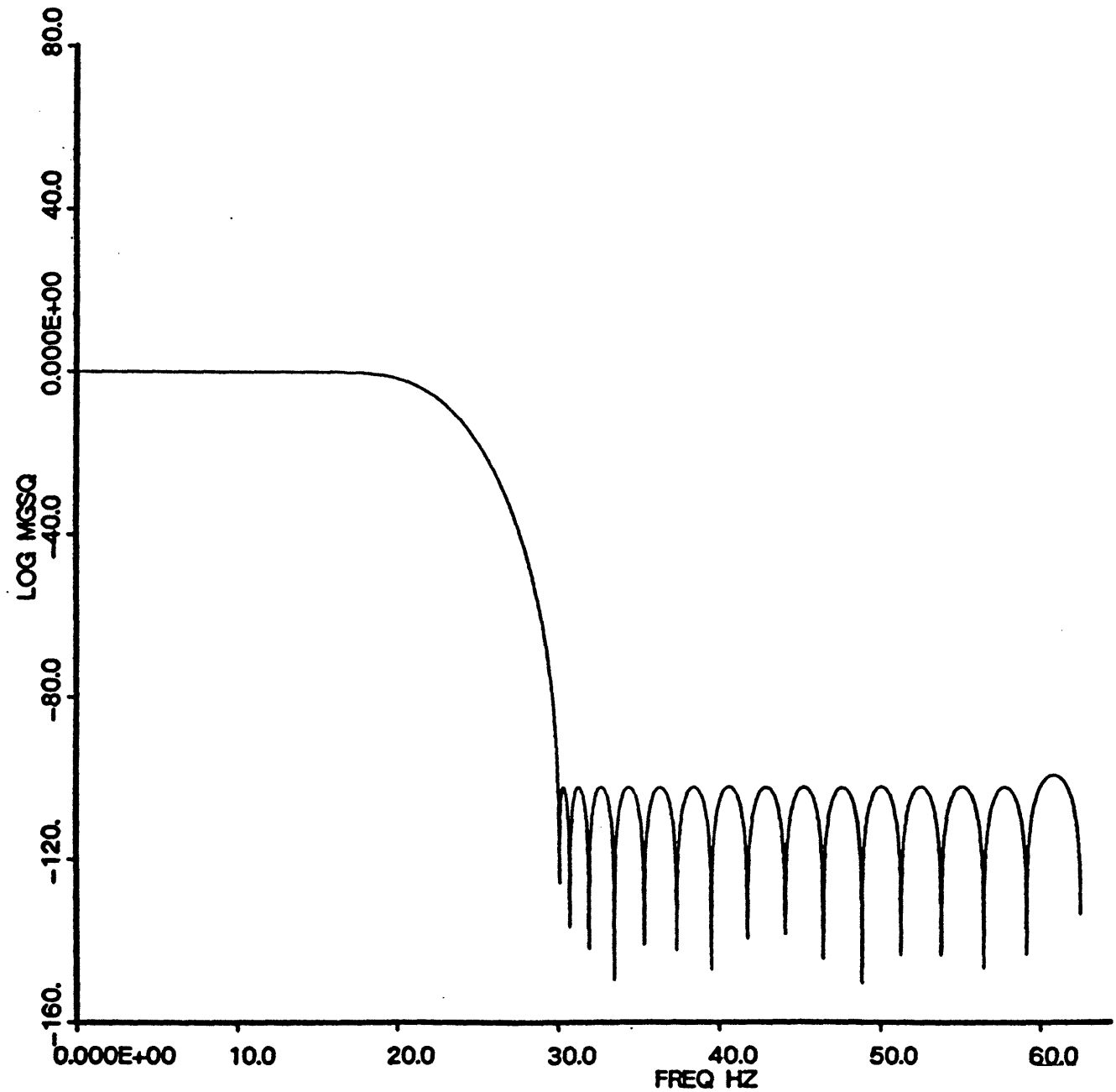

Figure 6. Experiment 1: Low Pass Filter.

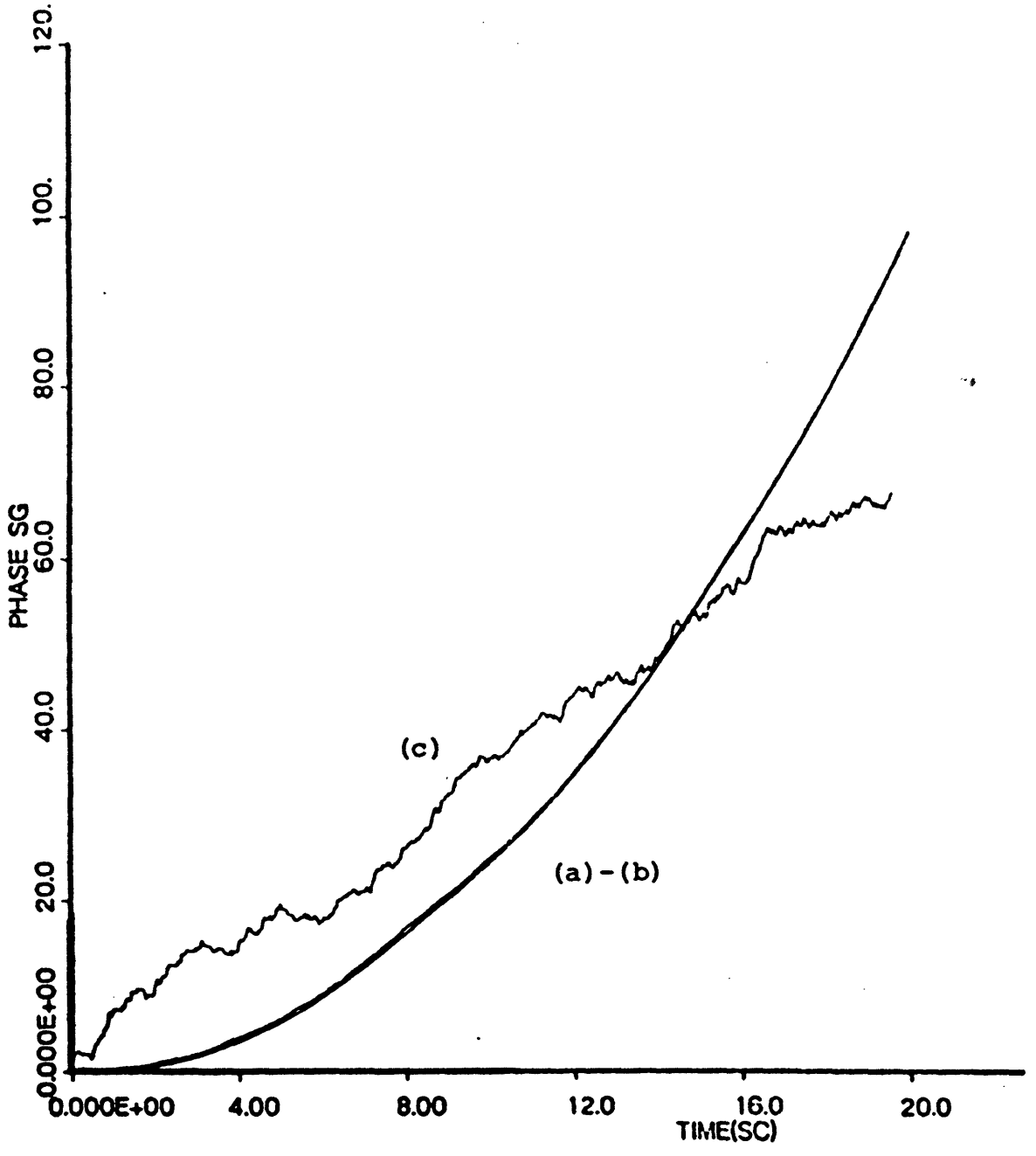

Figure 7. Experiment 1: Phase
(a) True Process
(b) Statistical Phase Unwrapper Estimate
(c) Atan Phase Unwrapper Estimate.

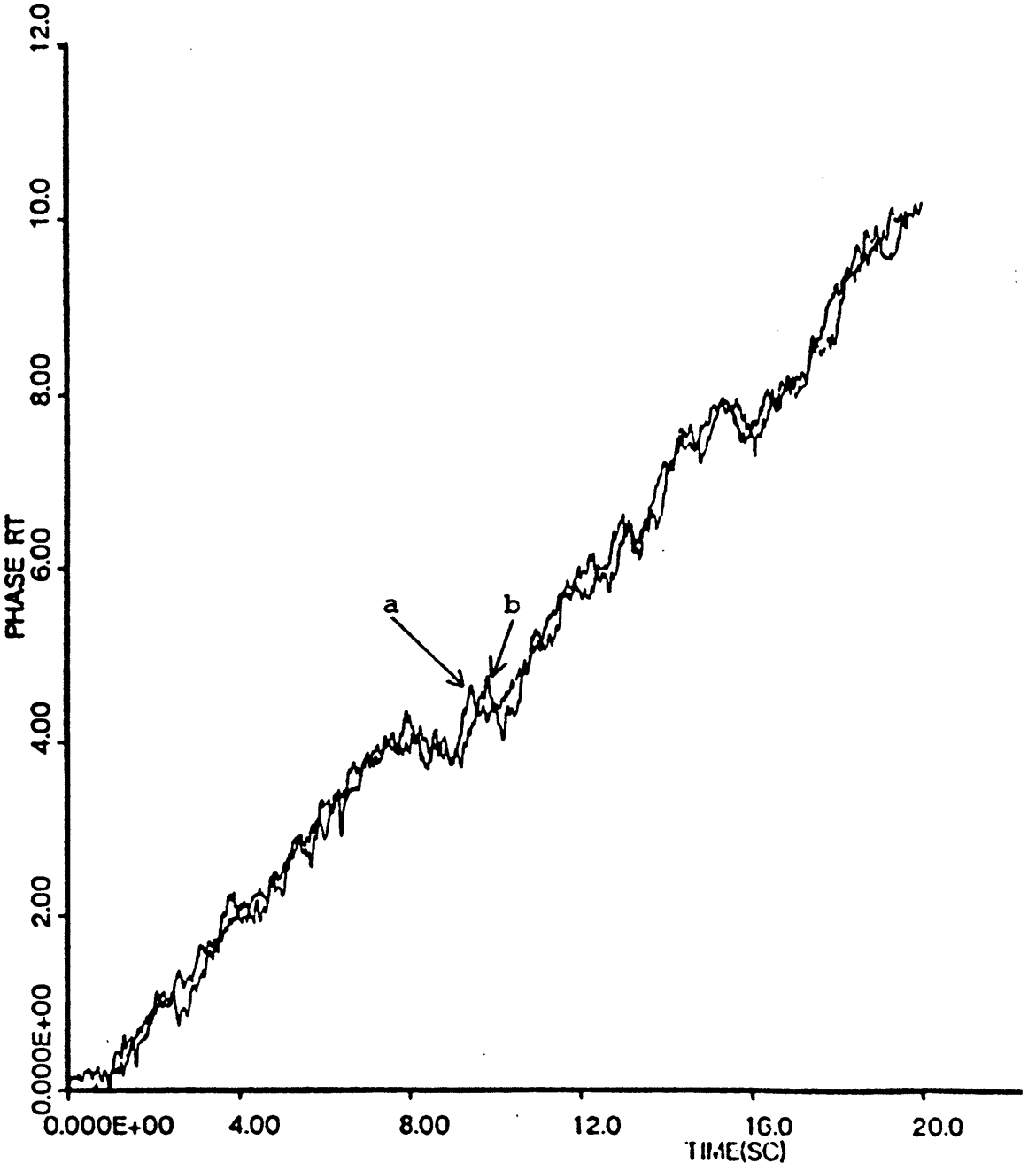

Figure 8. Experiment 1: Phase Rate
(a) True Process
(b) Statistical Phase Unwrapper Estimate.

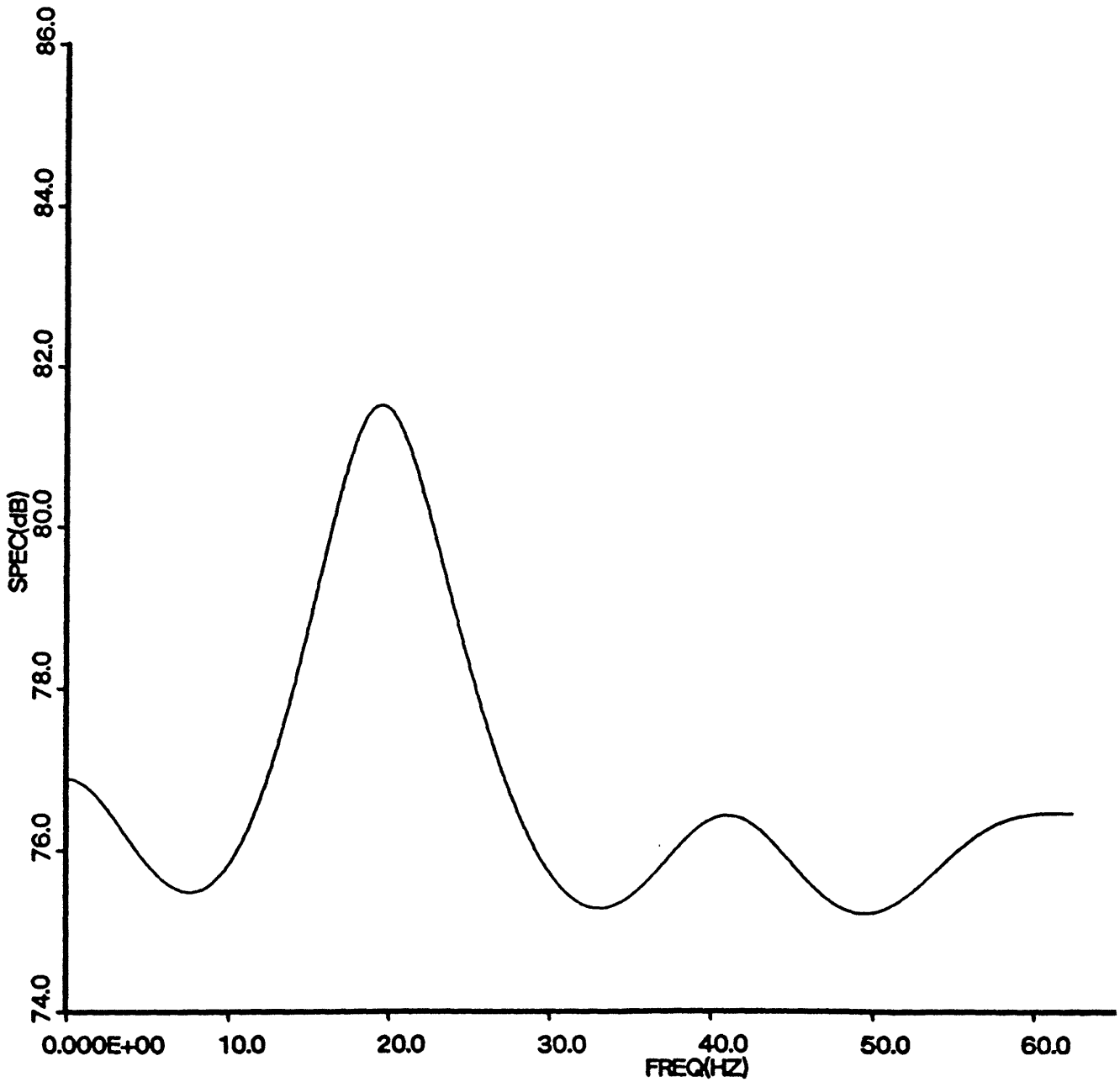

Figure 9. Experiment 2 ($f_0 = 15\text{Hz}; q = 0.5; r = 5 \times 10^{-9}$): Burg Spectral Estimate (10 poles).

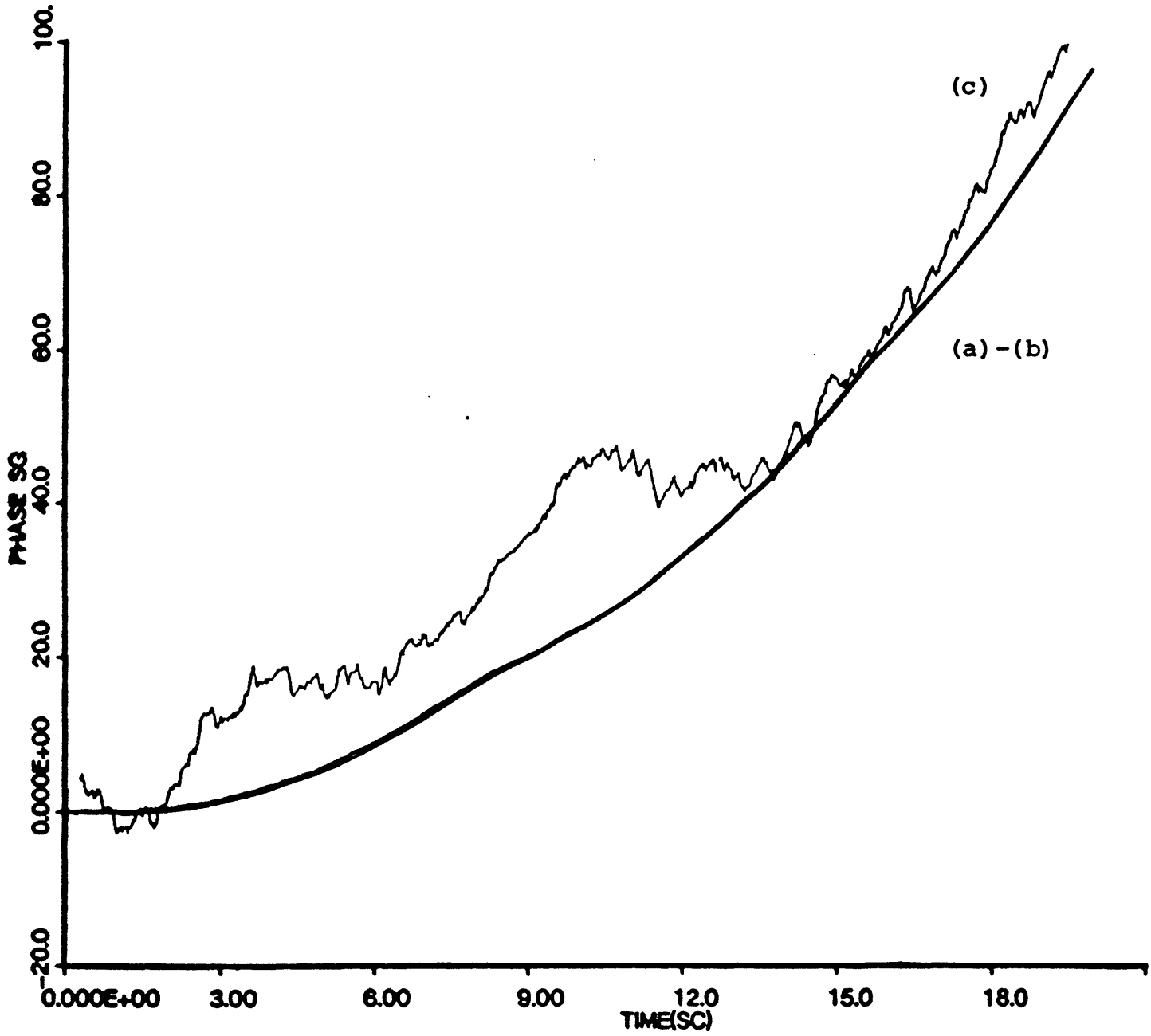

Figure 10. Experiment 2 ($f_0 = 15\text{Hz}; q = 0.5; r = 5 \times 10^{-9}$):
Phase

(a) True Process
(b) Statistical Phase Unwrapper Estimate
(c) Absolute Phase Unwrapper Estimate.

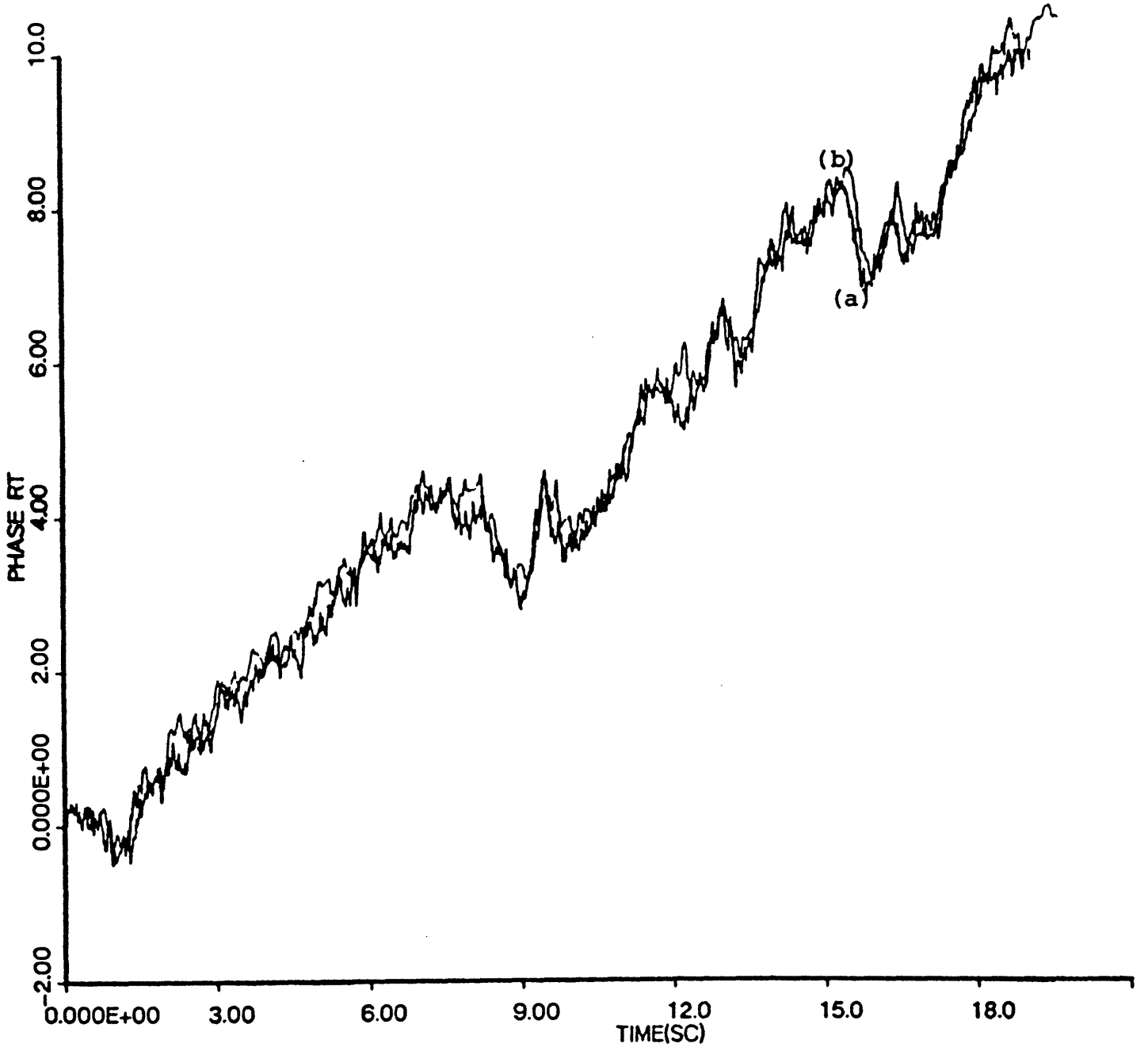

Figure 11. Experiment 2: Phase Rate
(a) True Process
(b) Statistical Phase Unwrapper Estimate.

determined by the prior statistics assumed. Said in other words, when the signal is present, to a large extent, the SPW is insensitive to offsets in the parameters' values, filtering being the dominant mode. When the signal is absent, the model assumed in the design of the SPW no longer is in accordance with reality, prediction prevailing over the behavior of the SPW. In a real world application, this behavior can be used to test for inconsistencies between the model and the physical system.

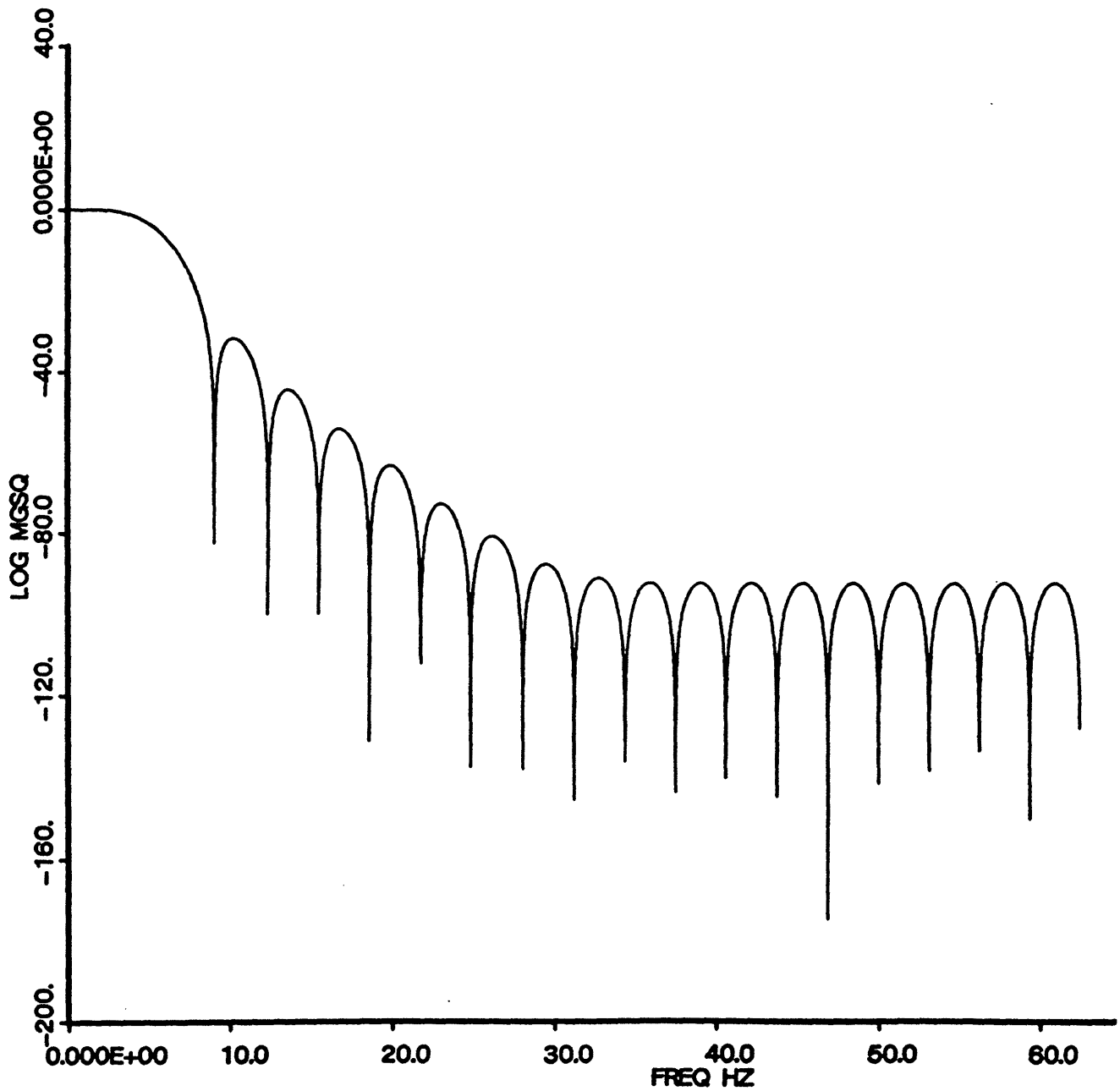

Figure 12. Experiment 3: Low Pass Prefilter.

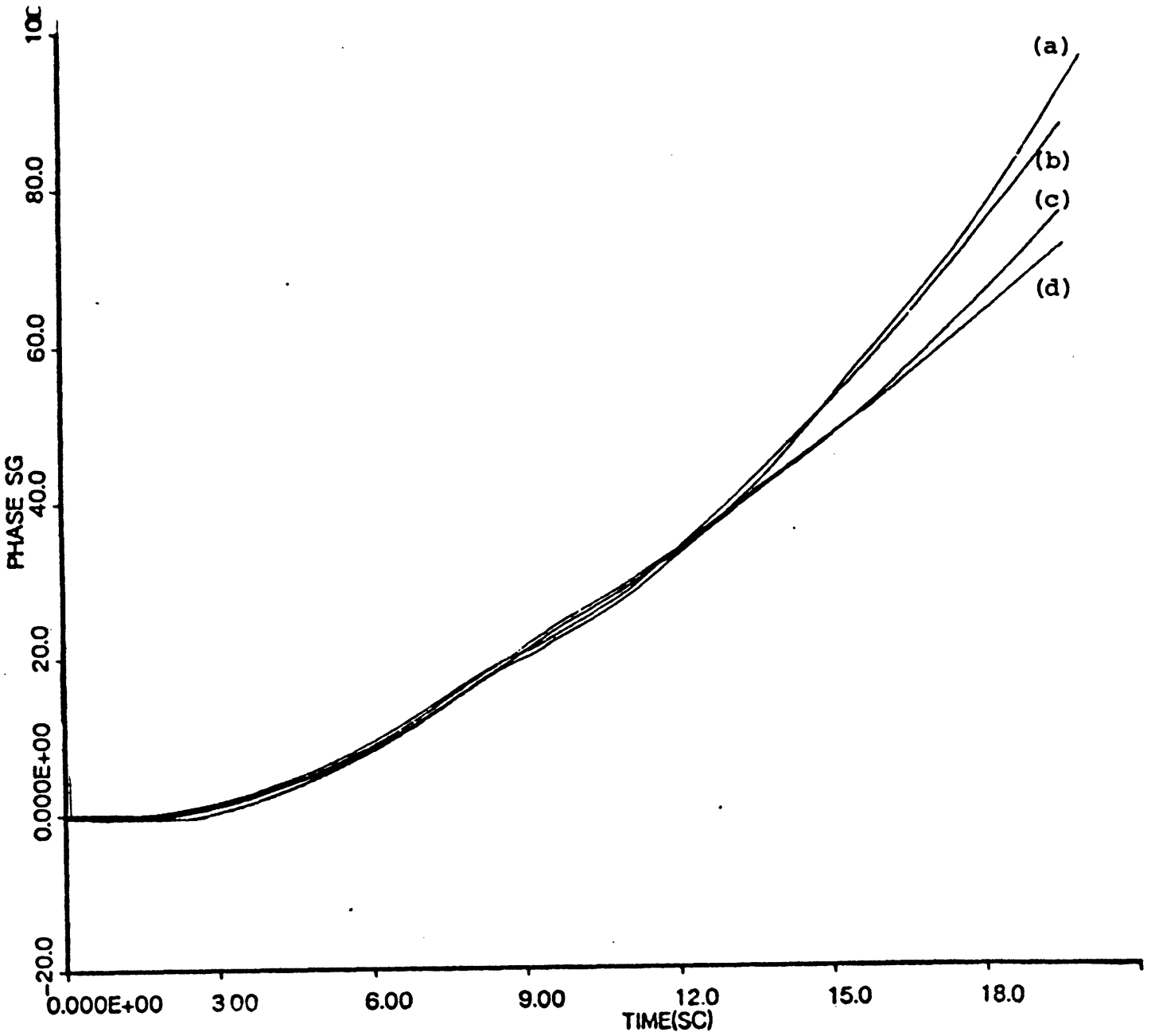

Figure 13. Experiment 3 ($f_0 = 15\text{Hz}; q = 0.5; r = 5 \times 10^{-8}$):
Phase

(a) True Process
(b) Statistical Phase Unwrapper ($\alpha_0 = 0.3, q = 2.0$)
(c) Statistical Phase Unwrapper ($\alpha_0 = 0.3, q = 0.2$)
(d) Statistical Phase Unwrapper ($\alpha_0 = 0.2, q = 0.2$).

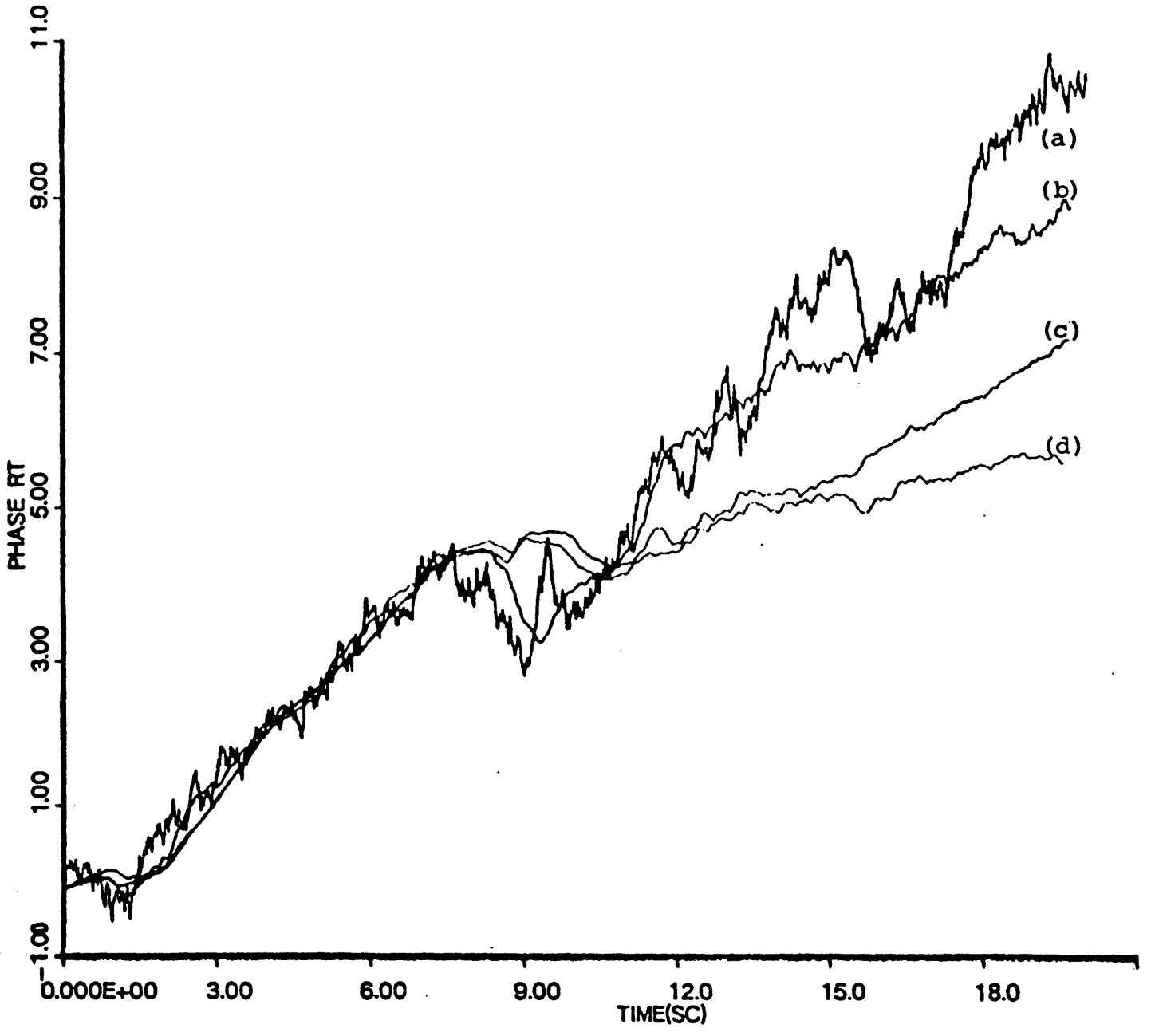

Figure 14. Experiment 3: Phase Rate
(a) True Process
(b) Statistical Phase Unwrapper ($\alpha_0 = 0.3, q = 2.0$)
(c) Statistical Phase Unwrapper ($\alpha_0 = 0.3, q = 0.2$)
(d) Statistical Phase Unwrapper ($\alpha_0 = 0.2, q = 0.2$).

7. Processing of the Arctic Data

Recalling from section 2, the signals to be analysed were generated by a highly stabilized cristal source vibrating at a nominal 15 Hz frequency. They propagated about 300 km being received by a 24 channel L-shaped array with leg span of 800 m. The sampling rate of digitization was 250 Hz. The receiving system response rolling off at 80 Hz, this is well above the Nyquist rate. The basic steps of the processing are summarized in figure 15.

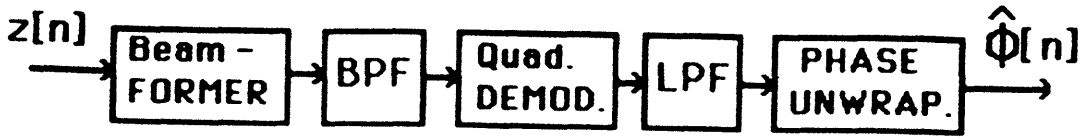

Figure 15. Arctic Data Block Processing.

In [14], the structure of figure 15 was used, with intermediate stages of decimation applied. The filters were FIRs of 500 sample points duration. After sufficient decimation, the final LPF had a band pass of 128 mHz centered on the demodulated tone. This processing reduced significantly the noise induced fluctuations on the phase process, the arctan providing a highly stabilized phase path. There were observed, however, unexplained peaks of very short duration. Identification of these fast events with the well known cycle slip phenomena associated with phase unwrappers, see [17], [18], is precluded because they did not correspond to an integer multiple of cycles, but rather to a fraction of a cycle. Physical considerations make it unlike that such fast phenomena were due to the temporary anihilation of a strong signal path.

To diagnose if they are or are not artifacts of the processing, it is important to process the data of individual hydrophones, and to use shorter FIRs, the latter requiring larger filter bandwidths. In either case, the noise to signal power ratio is increased, the arctan phase unwrapper (APW) looses track, the spikes are masked by the rapid succession of cycle slips. The stochastic phase unwrapper (SPW) of sections 4 and 5 is here applied. The data analysis pursued corresponded to several versions of the sequence described in figure 15. For the sake of brevity, only a representative set is reported here. It conveys and is supportive of the general conclusion provided by all the experiments that were carried out. Both beamformed and individual sensors' data are studied. The analysis detailed below focuses on an interval of 150 s about the first spike identified in log 4, figure 12 of [14], here reproduced for illustration purposes in figure 16a. Figure 16b, also of [14], shows

the corresponding amplitude fades. The second spike of the same log was also the subject of study, identical conclusion about its nature being reached.

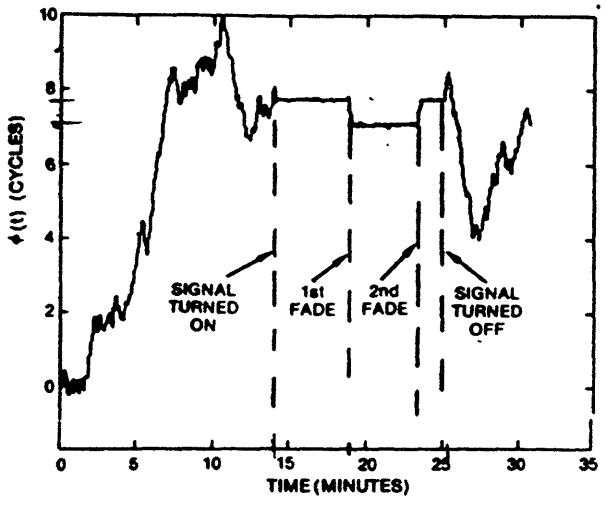

Figure 16a. Phase Path in Experiment 4 of [14].

To help with the identification of the main features of the received signals, Burg spectral estimates are constructed, see figure 17, for the beamformed Burg spectrum (160 poles). Besides the low frequency contents deriving from struming and array vibration, one distinguishes in a background of wideband noise, the tone of interest at 15 Hz, and a vestigial 60 Hz power component. The band pass filter (BPF) and the low pass filter (LPF) of the schema in figure 15 were designed via the Remez-Exchange algorithm. The BPF is centered at 15 Hz with a passband of 10 Hz, see figure 18a. The LPF has a halfbandwidth of 5 Hz, see figure 18b. The filters' impulse responses have equivalent durations of 50 points. Decimation with a factor of 2 was used only before LPF, so that the FIRs of both filters are respectively 200 msec and 400 msec. This is much smaller than the duration of the spike, being then possible to rule out unlike but possible rare events like loss of a clock pulse in the recording equipment.

Application of SPW requires a suitable statistical model. The phase process of the tone generated by the cristal is taken as a second order linear process (see section 4, or in section 6 take $\alpha_0 = 0$), the narrowband signal being assumed a pure sinusoidal carrier, whose frequency is chosen at the receiving end as the peak of the Burg spectrum. An unintentional downward trend exhibited by the phase paths below is a result of a slight offset of this assumed value with respect to its

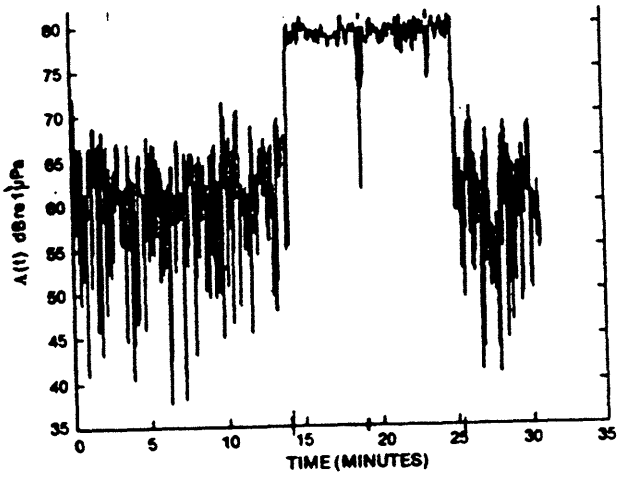

Figure 16b. Signal Amplitude in Experiment 4 of [14].

real value. The statistical parameters, namely q and r (see again section 6), are not known exactly. A reasonable estimate of the noise to signal ratio for the beamformed data can be obtained from [14]. Alternatively, it can be estimated from the Burg spectral estimates. From section 6, it is learned that the SPW is robust with respect to perturbations on the exact values of the parameters, and that if filtering is the dominant mode, the global behavior of SPW is not affected by these offsets. If the model misfit is too large, then, experiment 3, section 6, says that the SPW response is markedly different. The processing results are now examined.

The spike of concern is located about 250 s after the signal has been turned on in log 4. The data analysed corresponds to the interval [220 370] s. The origin of the time axes in all figures is relative to the lower end of this interval. Figures 19 to 21 concern the beamformed data. Figure 19 shows the phase path reconstructed by the SPW, while figure 20 displays the corresponding APW curve. The latter provides no clues, the spikes masked by the rapid succession of slips. At the SPW output, it is readily apparent that on or after the 240 s time reference (0.4 min in the figures horizontal labelings), the phase slips down with a fast trend, to an apparent recovery, followed by a fast down trend again, finally locking on the slow global trend. The event lasts for less than 18 s. The burst is also apparent from the frequency rate path provided in figure 21. A rough evaluation of the total difference between the upper (left) and lower (right) downward dominant trends, before and after the spike, shows a loss of approximately 0.6 to 0.8 of a cycle. Being less than

1 cycle, it cannot be attributed to a temporary loss of lock of the type occurring in phase and frequency modulation systems, known as cycle skips.

Figures 22 to 27 repeat similar processing curves for the SPW and the APW tracks for individual sensors. Note the different vertical scales. In all pictures, at the same time frame (and discounting the relative delays between sensors), the presence of a similar spiky pattern is distinguished in the phase process and its rate. The corresponding APWs' curves are inconclusive. From sensor to sensor, the noise environment changes. In particular, in channel 10 the noise is much stronger than in other channels. By retuning the statistical parameters of the SPW, it is still possible to enhance the phase path, clean the noise, and exhibit the pattern of concern, see figure 24, where a blow of the SPW phase is presented.

With the same channel data, and repeating for each individual channel, the SPW was tuned at alternative sets of parameters, consistently obtaining the same spiky pattern. The insight provided by experience 3, section 6, justifies the conclusion that this impulsive event is an intrinsic feature of the recorded data, and that it is not artificially introduced by the processing. We can only speculate on its real causes: either one path becoming temporarily dominant, or a glitch showing in the source.

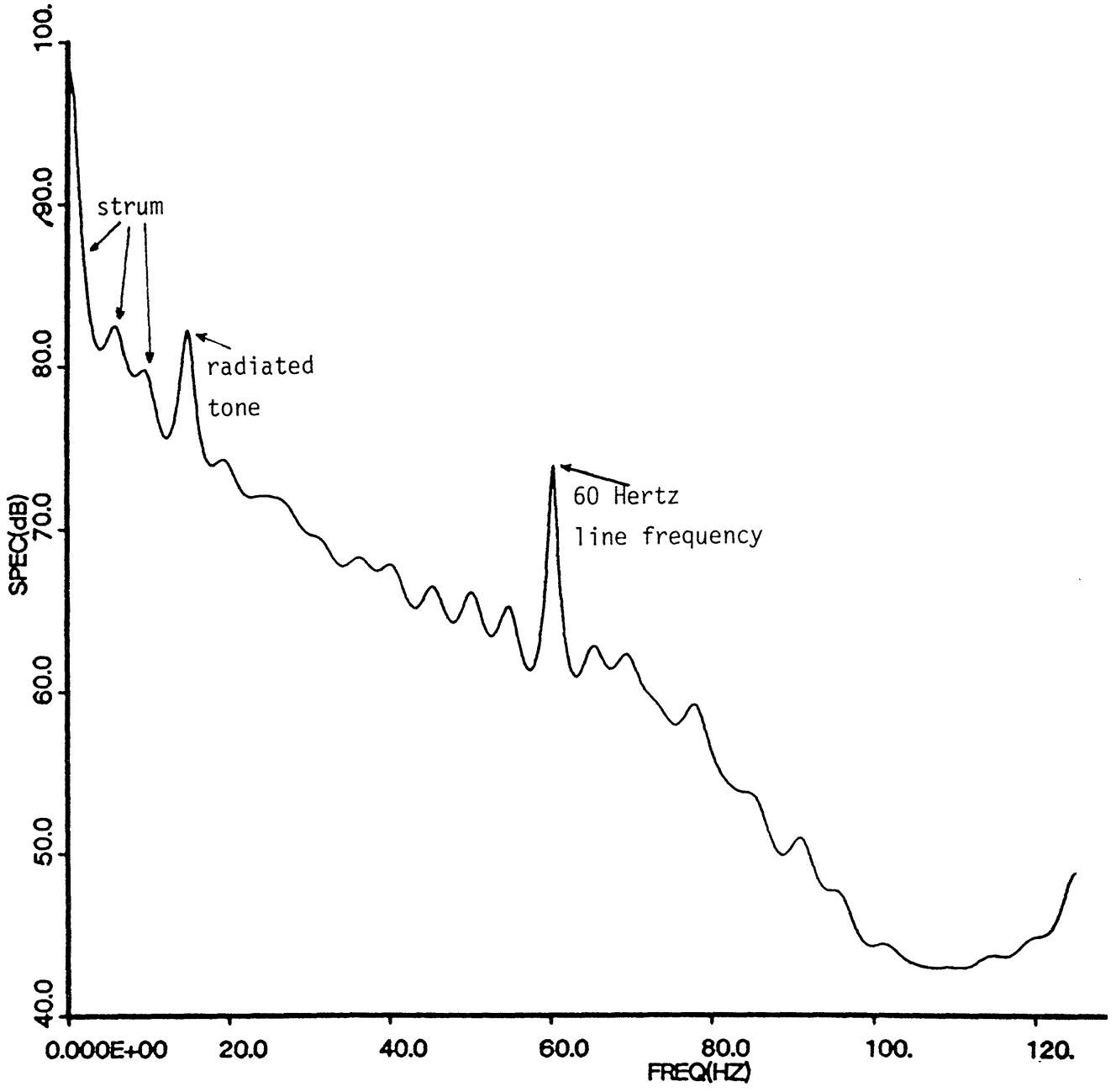

Figure 17. Burg Spectrum (160 poles): Beamformed Data.

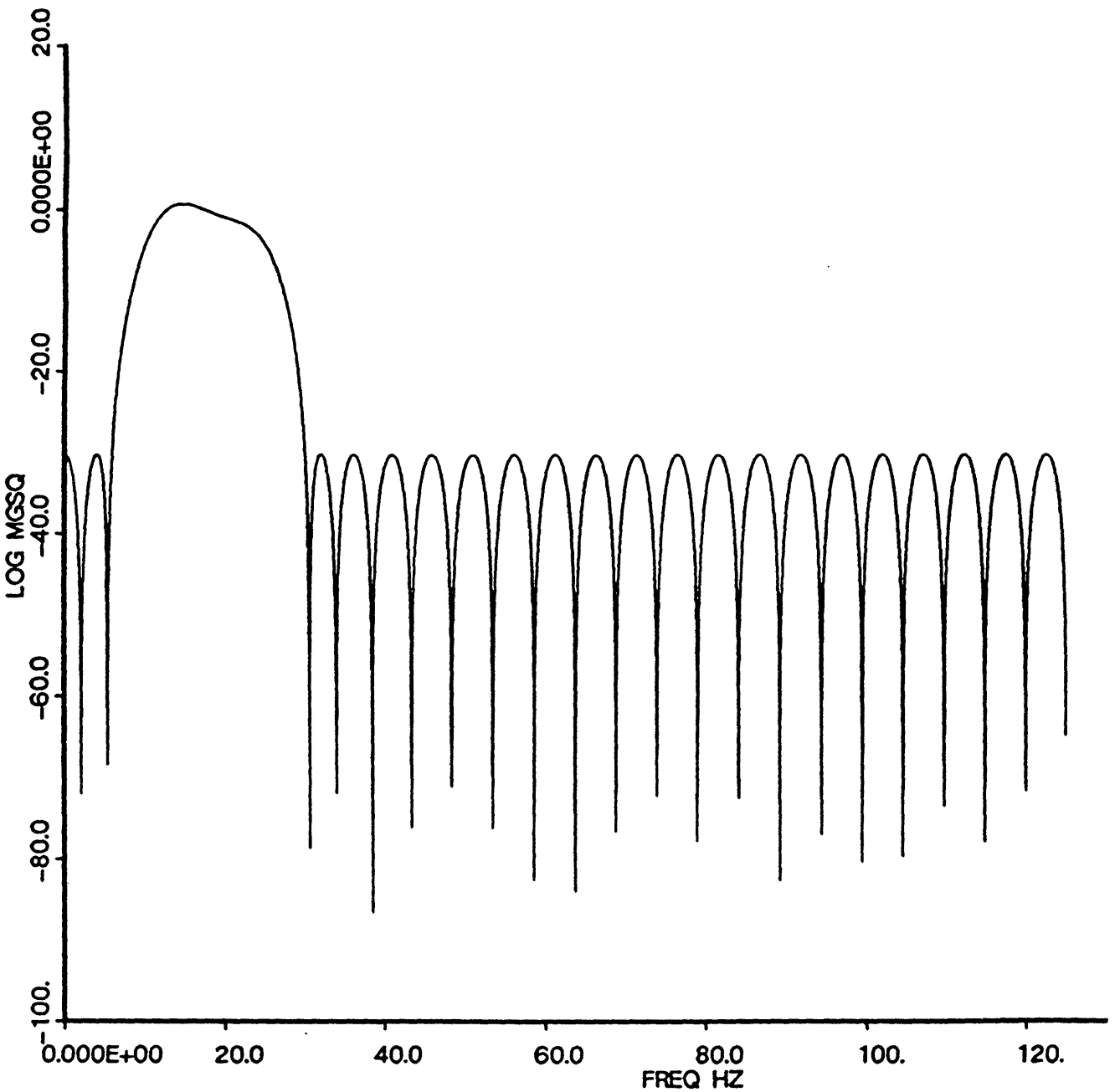

Figure 18a. Band Pass Filter: Frequency Response.

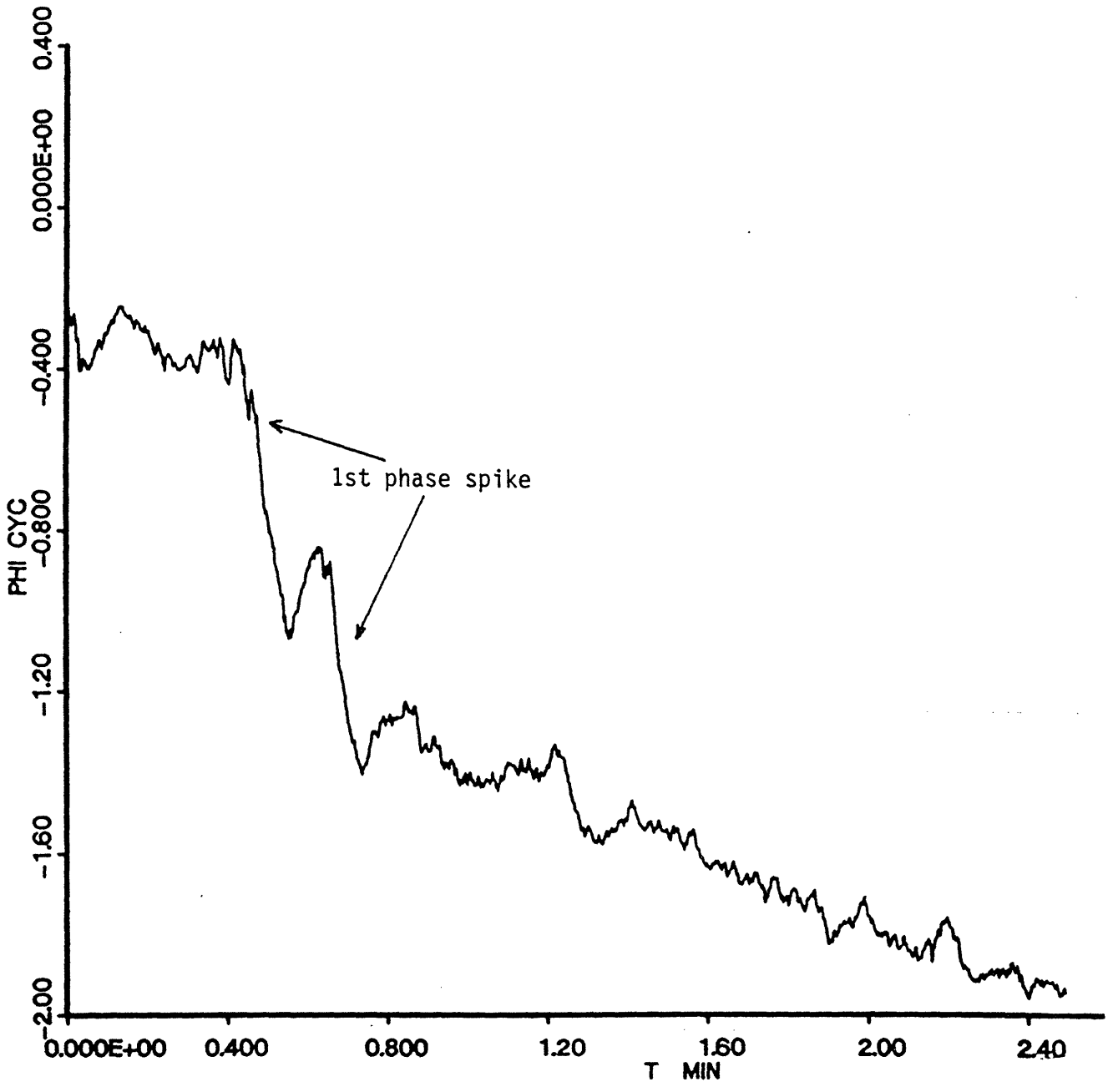

Figure 19. Statistical Unwrapper Phase: Beamformed Data.

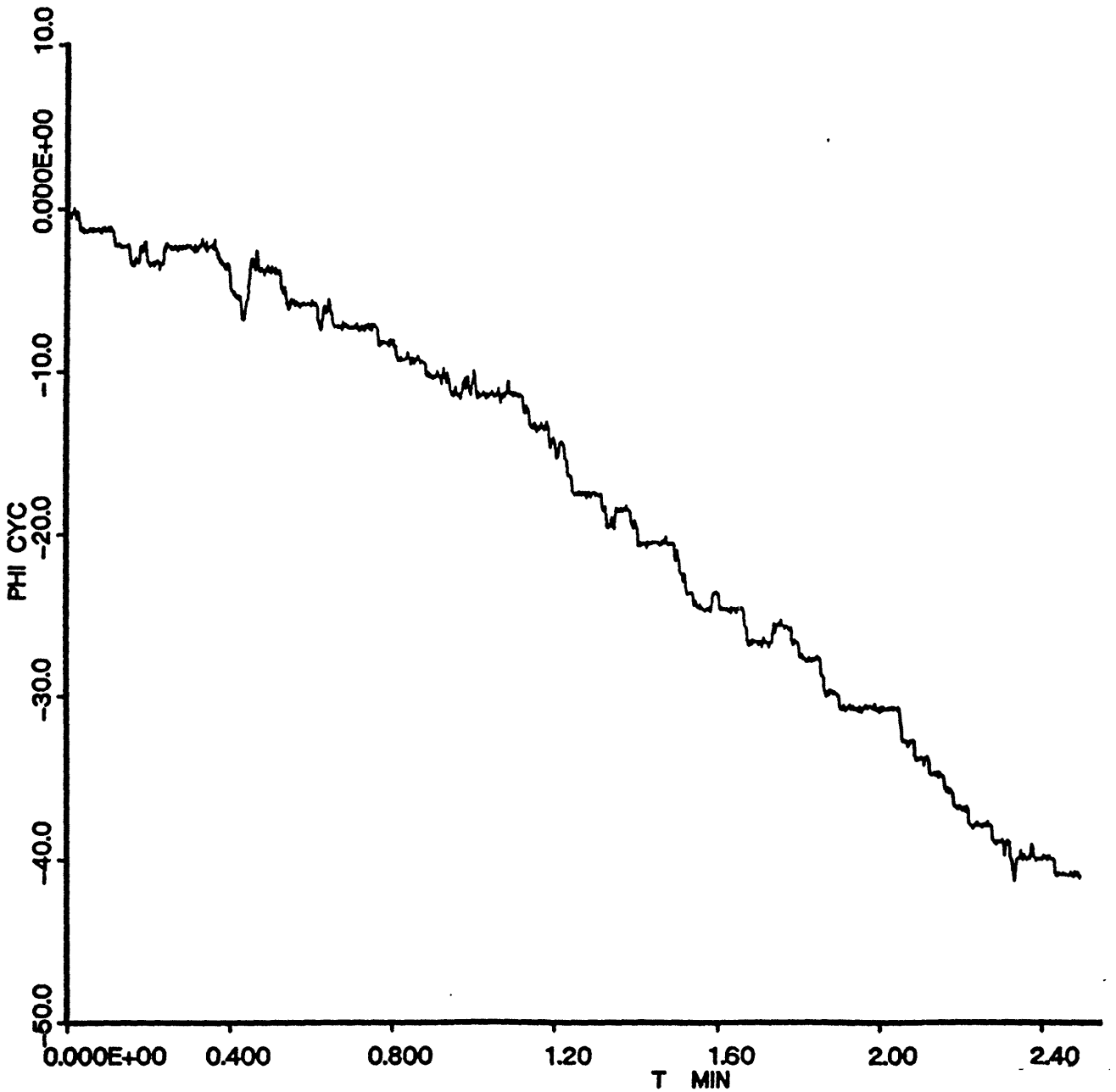

Figure 20. Atan Unwrapper Phase: Beamformed Data.

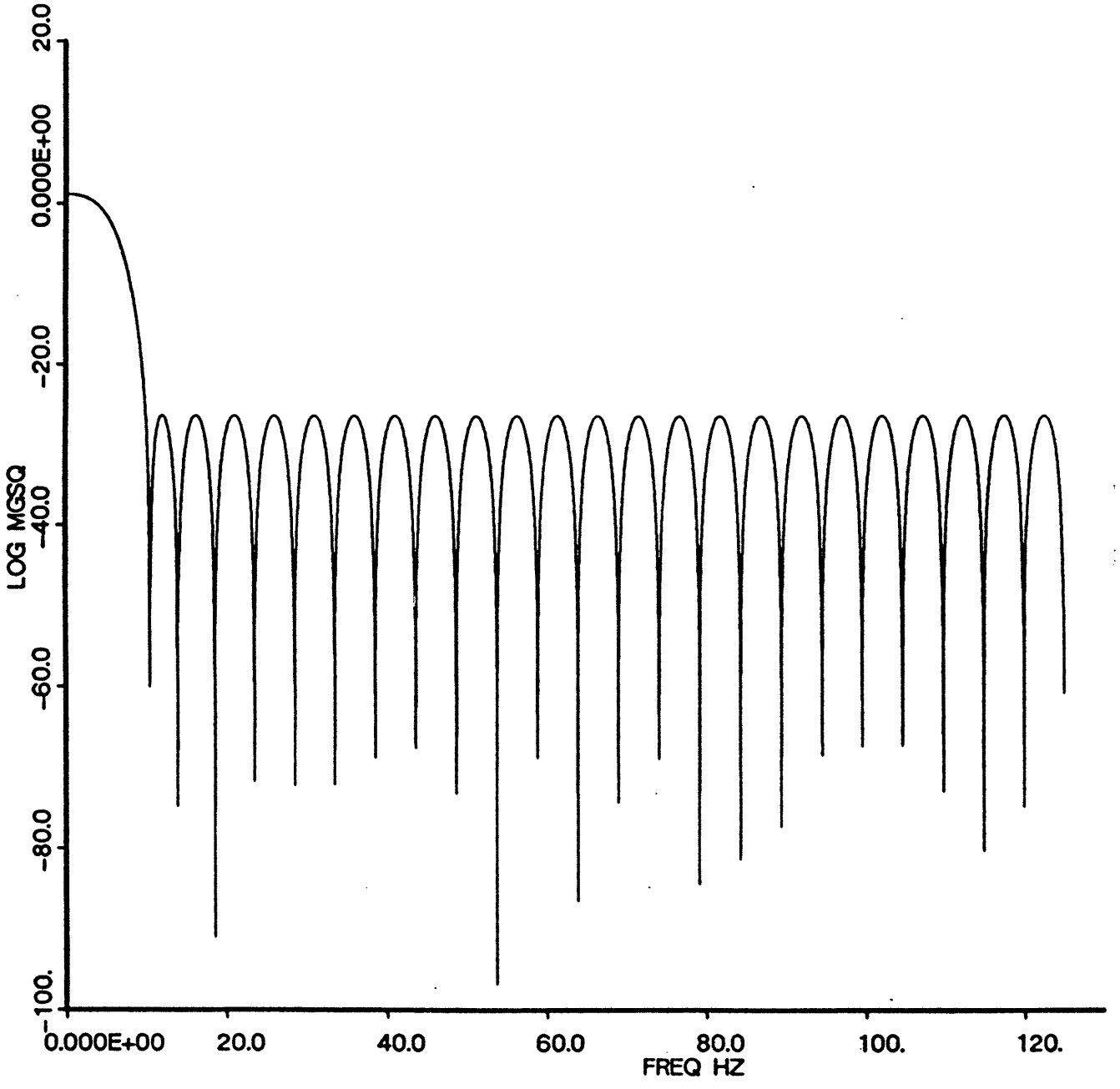

Figure 18b. Low Pass Filter: Frequency Response.

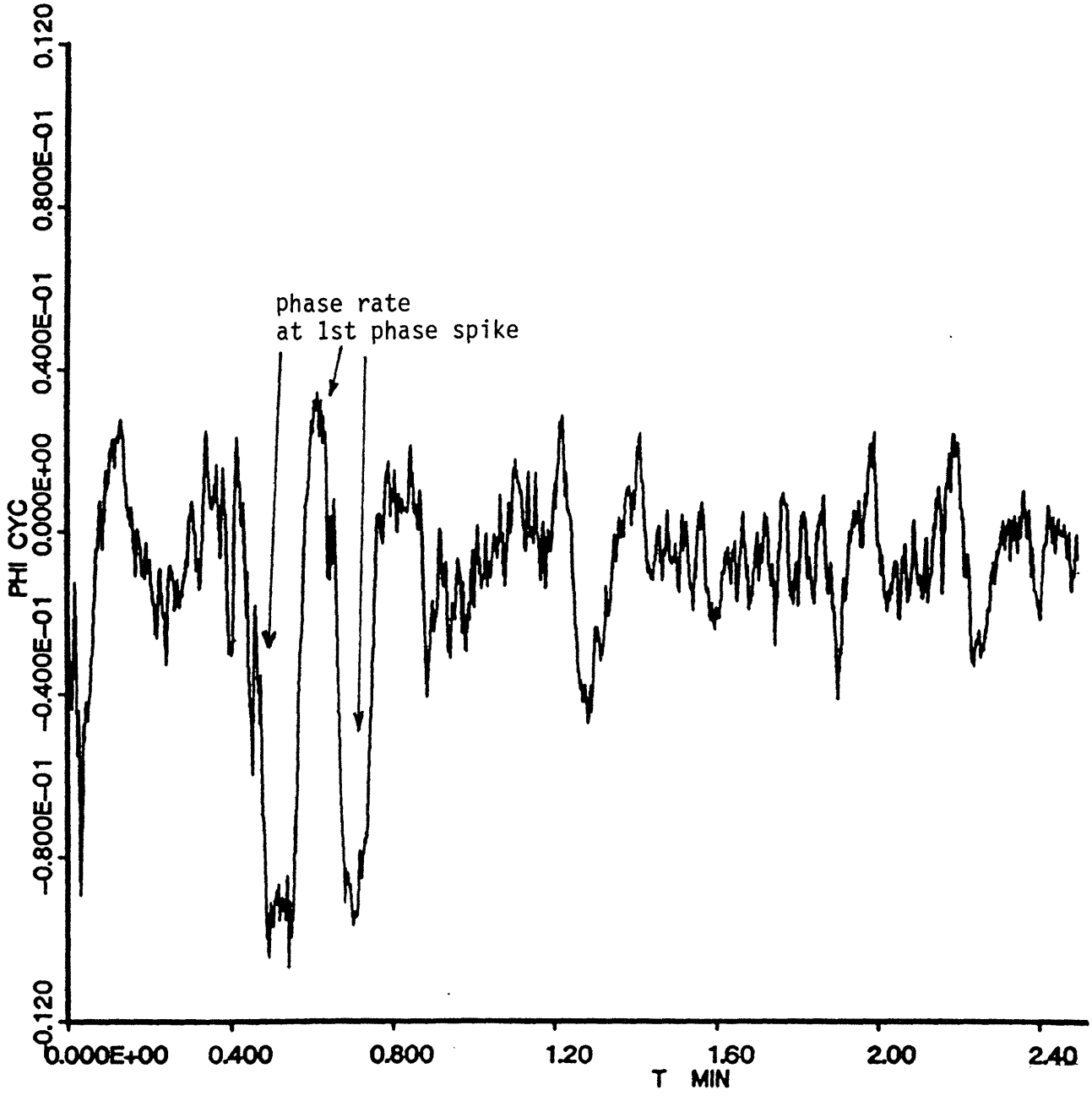

Figure 21. Statistical Unwrapper Phase Rate: Beamformed Data.

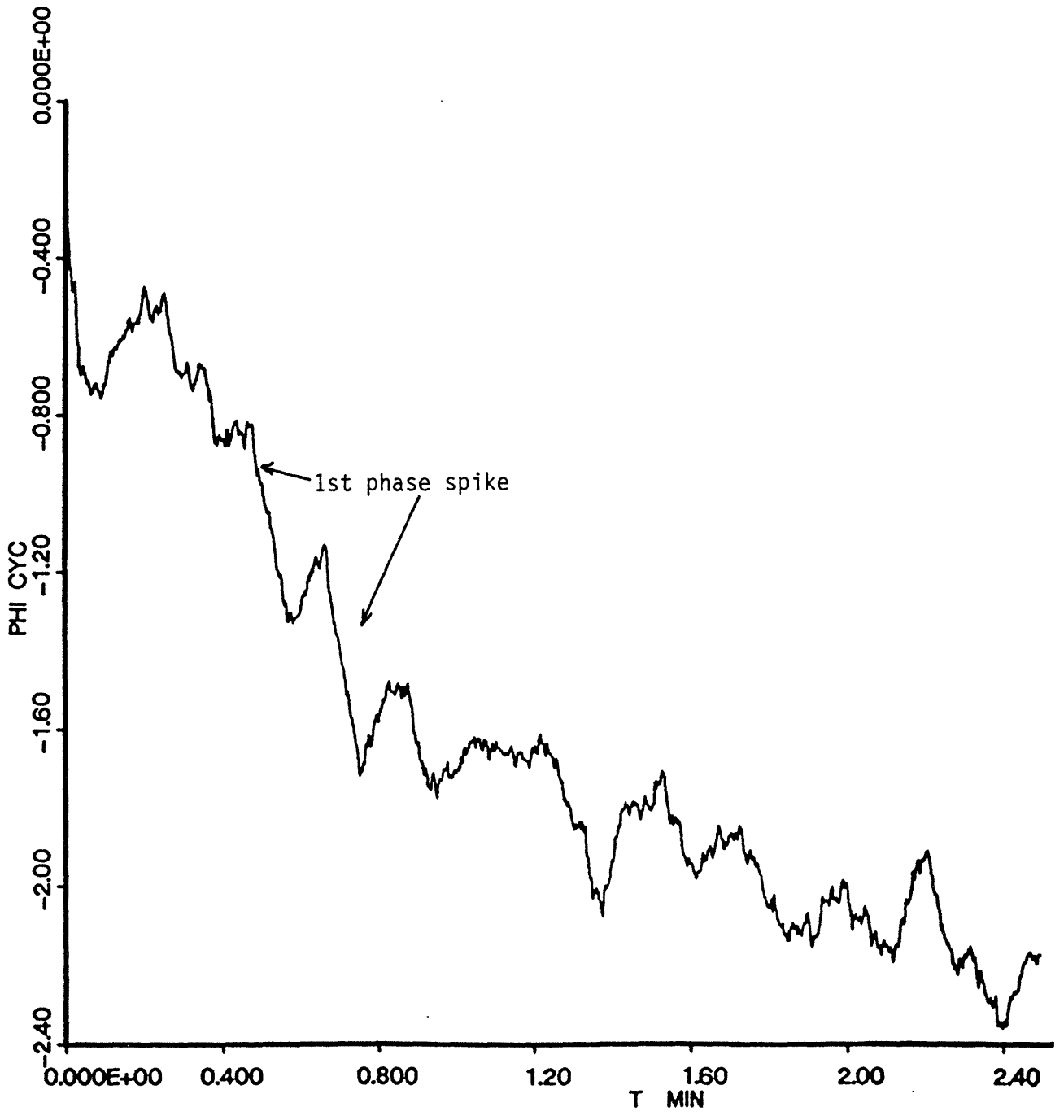

Figure 22. Statistical Unwrapper Phase: Channel 2 Data.

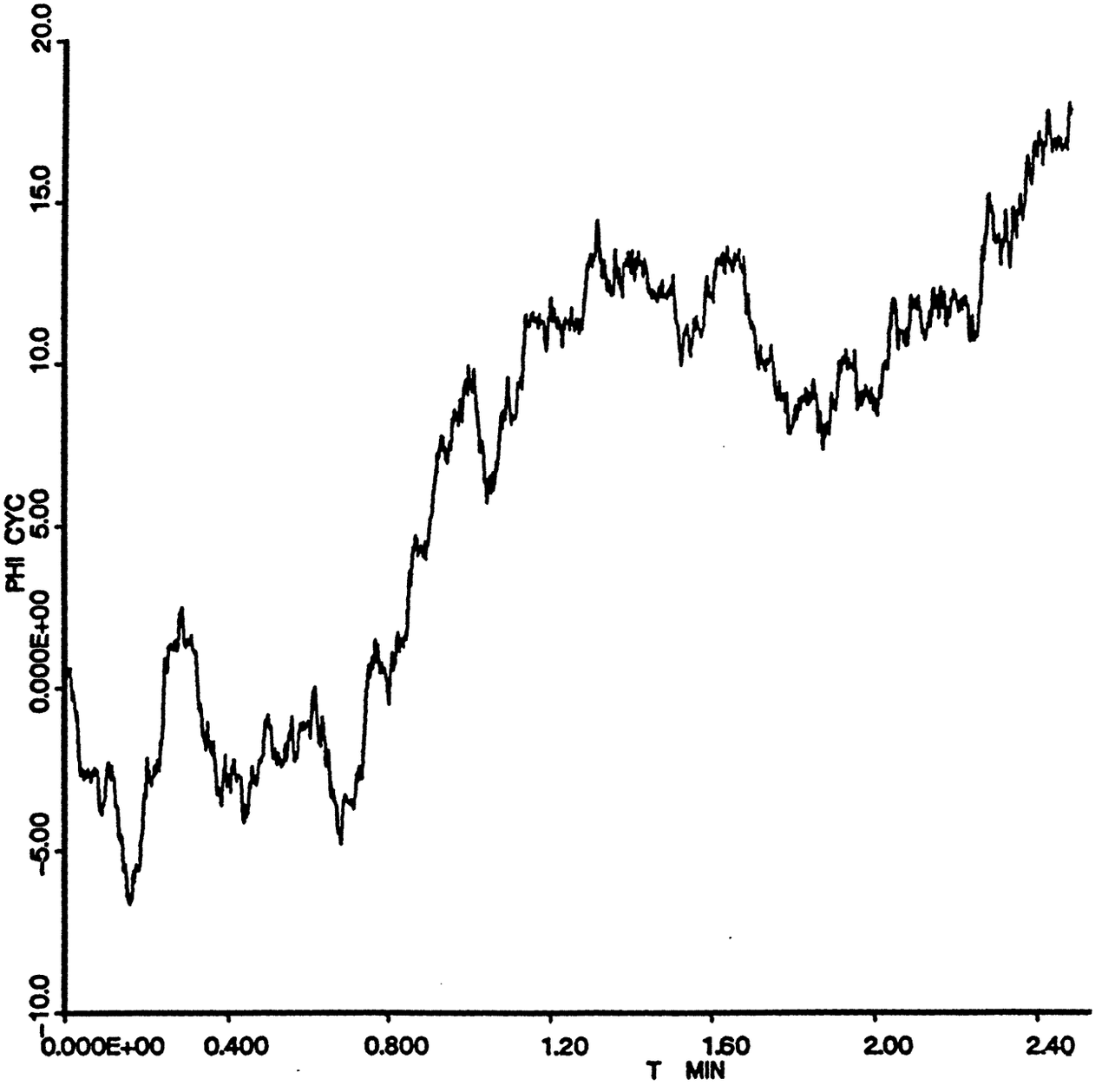

Figure 23. Atan Unwrapper Phase: Channel 2 Data.

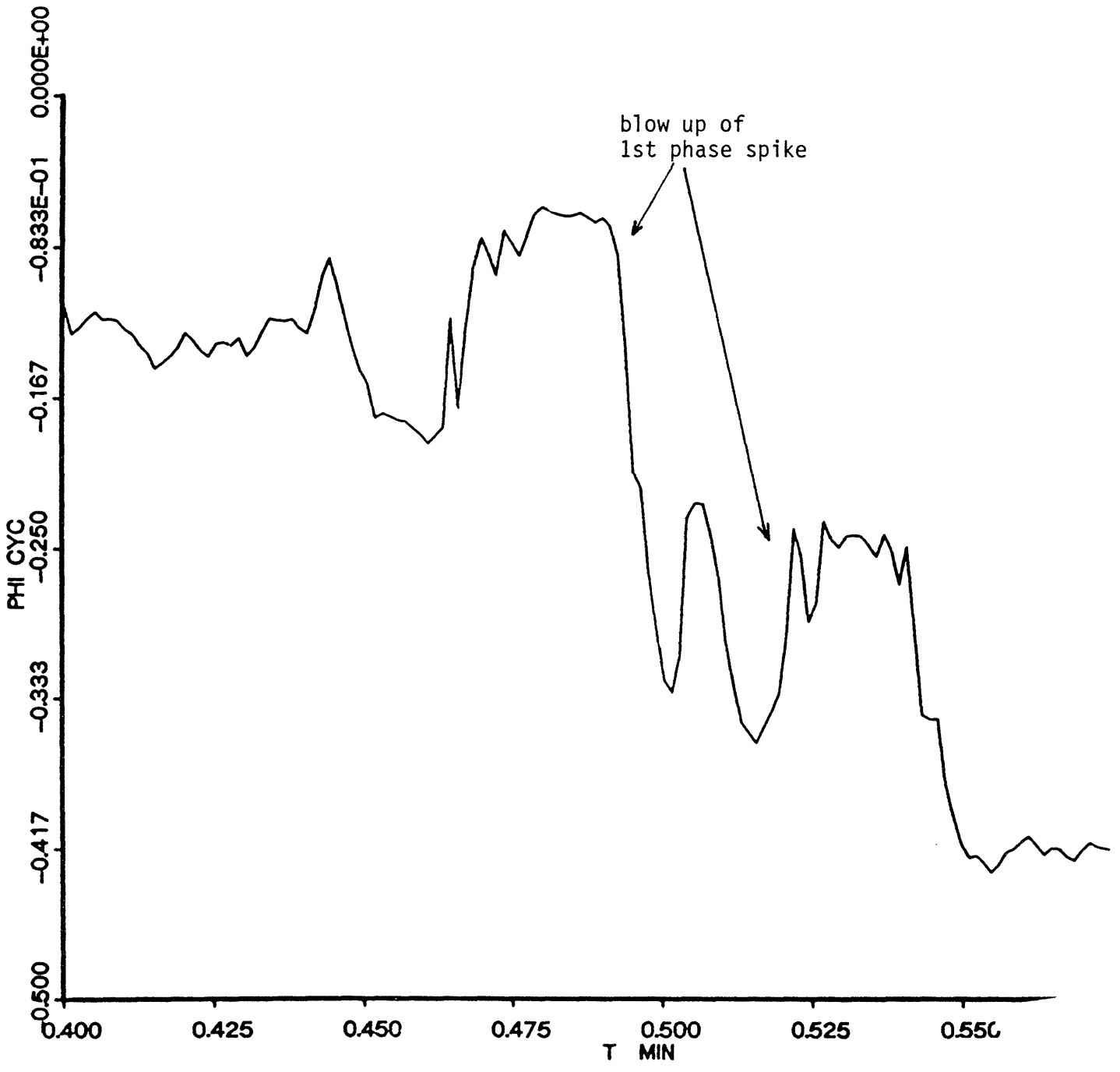

Figure 24. Statistical Unwrapper Phase: Channel 10 Data (Blow).

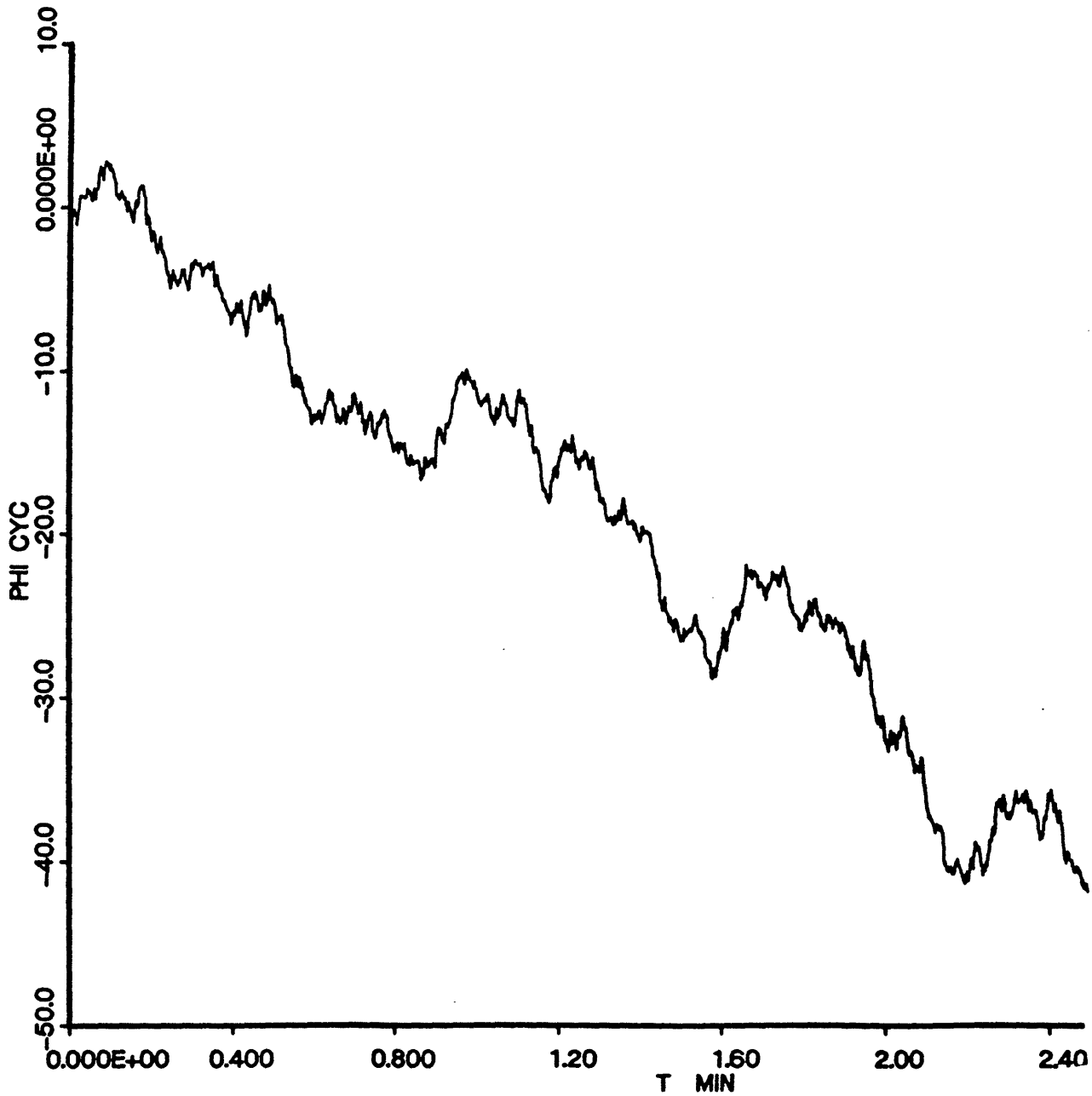

Figure 25. Atan Unwrapper Phase: Channel 10 Data.

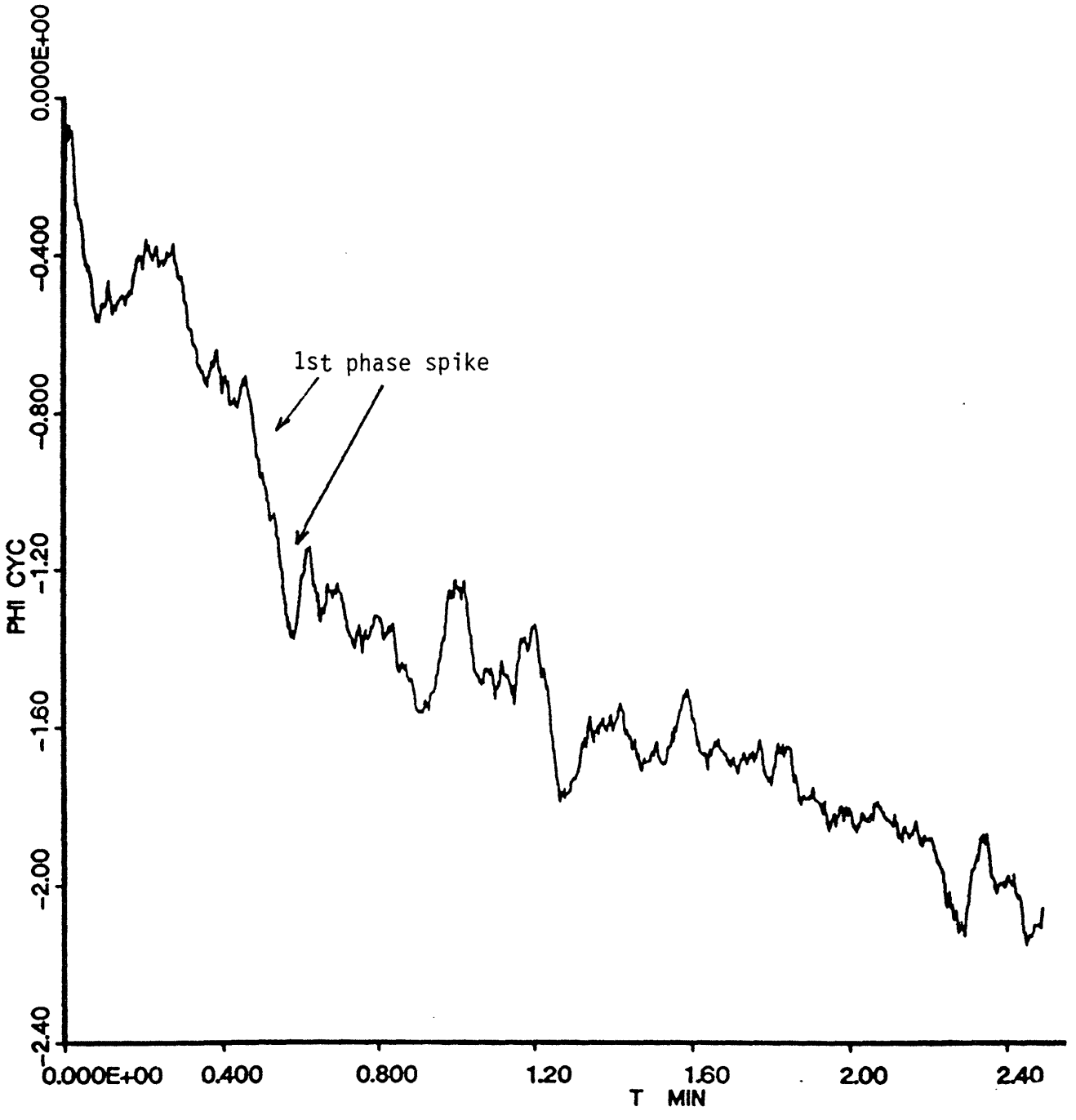

Figure 26. Statistical Unwrapper Phase: Channel 20 Data.

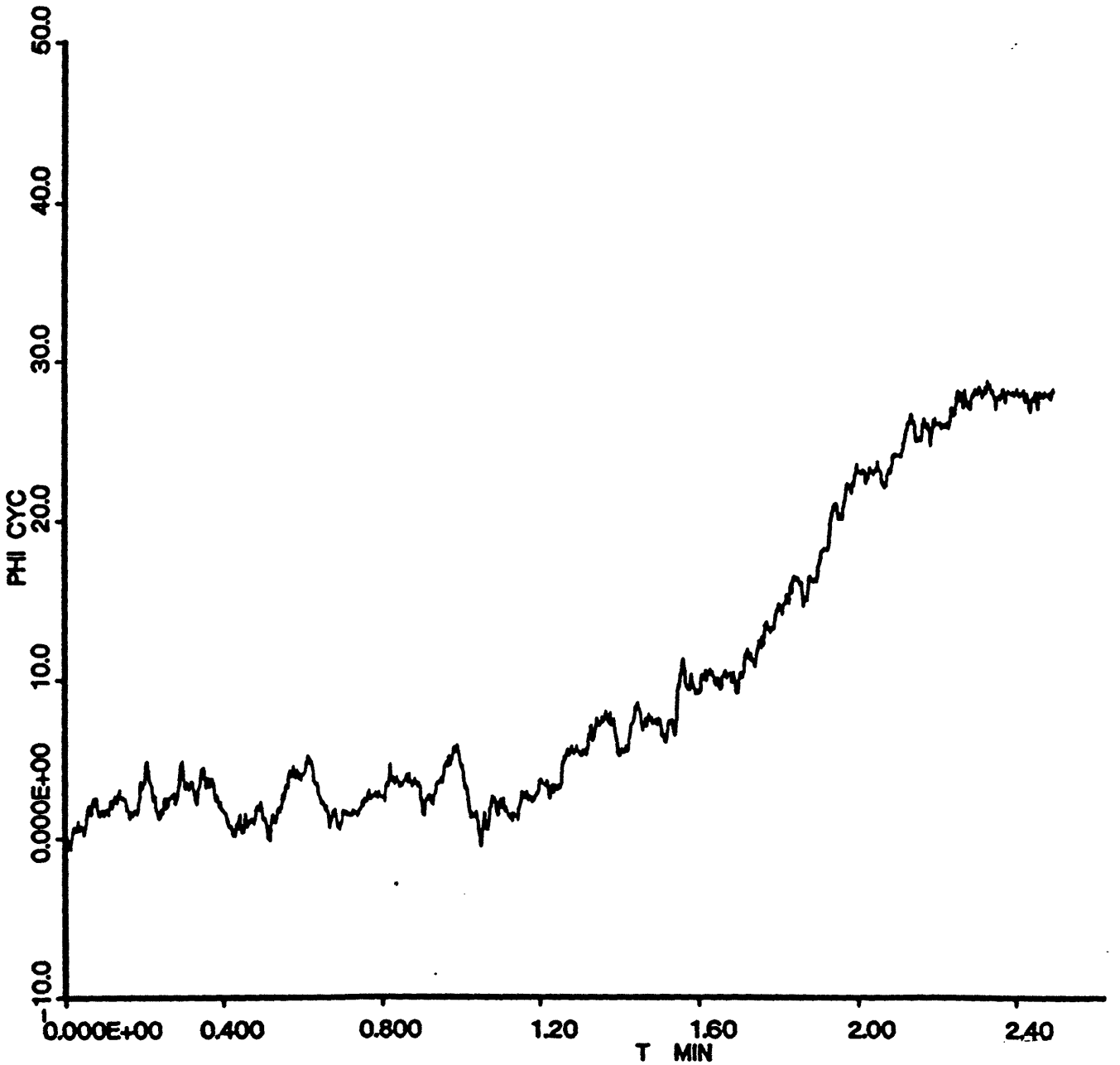

Figure 27. Atan Unwrapper Phase: Channel 20 Data.

Conclusion

The following are relevant issues drawn from the work described:

- An alternative to the phase unwrapping of time sequences was presented, designed via the techniques of stochastic nonlinear filtering theory. Taking into consideration the noisy nature of the phase instability and of the measurements disturbances, a reliable unwrapping is achieved.
- The statistical phase unwrapper (SPW) performance is dependent on the nature of the misfits between the model underlying the design and the real world data. Errors resulting from offsets of the assumed parameter values affect the local behavior but do not imply global divergence between the responses of differently tuned SPWs processing the same real data. Errors corresponding to basic misadjustments between the model assumptions and the real world translate into lasting long term effects in the SPW response, with each differently tuned SPW exhibiting its own distinct phase path (see section 6). With detuning errors, the SPW reacts dominantly in a filtering mode. With model mismatches, the predictive mode is prevalent in the SPW response.
- The previous remark says that the SPW is robust to parameter errors, and that it can be used to resolve fundamental inconsistencies between the model and the real physical system. This suggests that the nonlinear algorithm has a finite memory span, being able to switch between regions of operation, where in one greater reliance to new input data is given, and in the other greater emphasis is placed on the prior knowledge.
- Due to its robustness to imprecise knowledge of the parameters values, and to higher noise levels, the SPW supports more flexible preprocessing. The necessity of beamforming may be waived, and the prefilters required to clean the data may be designed with shorter responses and larger bandwidths.
- Application of the SPW to the Arctic data shows that the spiky pattern of concern is present in both beamformed and single sensors data, and when differently tuned SPWs run over the same data. The widely different conditions of operation (faster FIRs, beamforming and unbeamforming, largely different levels of noise to signal power ratios) leading sistematically to the same consistent global behavior support the conclusion that the impulsive behavior is not a processing artifact, rather it is an intrinsic characteristic of the recorded data. The exact origin, e.g., source transient, recording malfunctioning, is not clear. But, with high confidence, the SPW helps to rule out the demodulation processing as one of its causes.
- The work has described an application of nonlinear stochastic filtering theory to a real world problem. The flexibility provided by the SPW and its resistance to noise justifies its wider use in environments where the signal to noise power ratio is small, as typically happens in underwater acoustics.

Bibliography

[1] D. L. Alspach and H. W. Sorensen, "Nonlinear Bayesian Estimation Using Gaussian Sum Approximations," *IEEE Transactions on Automatic Control*, Vol. Ac-17, No. 4, Pp. 439-448, August 1982.

[2] A. B. Baggeroer and I. Dyer, "Fram 2 in the Eastern Arctic," *EOS Transactions Am. Geophys. Union*, April 6, 1982.

[3] A. B. Baggeroer and G. L. Duckworth, "Seismic Exploration in the Arctic Ocean," *Geophysics: The Leading Edge of Exploration*, pp. 22-27, October 1983.

[4] T. E. Bordley, "Phase Unwrapping of Symmetric, Anti-Symmetric Sequences," Ph. D. Thesis, Department of Electrical Engineering and Computer Science, Massachusetts Institute of Technology, 1985.

[5] R. S. Bucy and P. D. Joseph, "Filtering for Stochastic Processes with Applications To Guidance," Wiley Interscience, New York,1968; Chelsea, 1987.

[6] R. S. Bucy, F. Ghovanlou, J. M. F. Moura, and K. D. Senne, "Array Processing and Phase Modulation," *IEEE Computer Magazine*, invited paper, Special Issue on *Array Processing*, June 1983.

[7] R. S. Bucy and K. D. Senne, "Nonlinear Filtering Algorithms for Vector Processing Machines," *Computers and Mathematics with Applications*, Vol. 6, pp. 317-338, Pergamon Press, 1980.

[8] I. Dyer and A. B. Baggeroer, "The Fram 2 Experiment" *EOS Transactions Am. Geophys. Union*, Vol 61, No.6, 1980.

[9] R. E. Kalman and R. S. Bucy, "New Results in Linear Filtering and Prediction theory," *Trans. ASME, J. Basic Engrg.*, ser. D, vol. 83, pp. 95-108, 1961.

[10] J. M. N. Leitão and J. M. F Moura, "Nonlinear Filtering in Phase Acquisition," in *Signal Processing Theories and Applications*, eds. M. Kunt and F. de Coulon, N. Holland P. Co., pp. 437-442, 1980.

[11] J. M. N. Leitão, "Estimação Não Linear Óptima de Fase. Aquisição e Seguimento," Doctoral Dissertation, Department of Electrical and Computer Engineering, Instituto Superior Técnico, Lisbon, Portugal, February 1983.

[12] J. M. N. Leitão and J. M. F Moura, "Phase Demodulation: A Nonlinear Approach," to be submitted.

[13] R. McGowan and R. Kuc, "A Direct Relation Between a Signal Time Series and its Unwrapped Phase," *IEEE Transactions on Acoustics, Speech, and Signal Processing*, vol. 30, pp. 719-725, October 1982.

[14] P. Mikhaelevsky, "Characteristics of CW Signals Propagated Under the Ice in the Arctic," *J. Acoust. Soc. Am.*, vol. 70, no. 6, pp. 1717-1722, 1981.

[15] K. D. Senne, "A Machine Independent Random Number Generator," *Stochastics*, vol. 1, no. 3, pp. 3-23, 1973.

[16] H. L. Van Trees, "Detection, Estimation and Modulation Theory: Part I," John Wiley, New York, 1968.

[17] H. L. Van Trees, "Detection, Estimation and Modulation Theory: Part II," John Wiley, New York, 1971.
[18] A. J. Viterbi, "Principles of Coherent Communications," McGraw-Hill, New York, 1966.